Review article

Yan Pennec, Vincent Laude, Nikos Papanikolaou, Bahram Djafari-Rouhani, Mourad Oudich, Said El Jallal, Jean Charles Beugnot, Jose M. Escalante and Alejandro Martínez*

Modeling light-sound interaction in nanoscale cavities and waveguides

Abstract: The interaction of light and sound waves at the micro and nanoscale has attracted considerable interest in recent years. The main reason is that this interaction is responsible for a wide variety of intriguing physical phenomena, ranging from the laser-induced cooling of a micromechanical resonator down to its ground state to the management of the speed of guided light pulses by exciting sound waves. A common feature of all these phenomena is the feasibility to tightly confine photons and phonons of similar wavelengths in a very small volume. Amongst the different structures that enable such confinement, optomechanical or phoxonic crystals, which are periodic structures displaying forbidden frequency band gaps for light and sound waves, have revealed themselves as the most appropriate candidates to host nanoscale structures where the light-sound interaction can be boosted. In this review, we describe the theoretical tools that allow the modeling of the interaction between photons and acoustic phonons in nanoscale structures, namely cavities and waveguides, with special emphasis in phoxonic crystal structures. First, we start by summarizing the different optomechanical or phoxonic crystal structures proposed so far and discuss their main advantages and limitations. Then, we describe the different mechanisms that make light interact with sound, and show how to treat them from a theoretical point of view. We then illustrate the different photon-phonon interaction processes with numerical simulations in realistic phoxonic cavities and waveguides. Finally, we introduce some possible applications which can take enormous benefit from the enhanced interaction between light and sound at the nanoscale.

Keywords: light-sound interaction; photonic crystals; phononic crystals; optomechanical crystals; cavity optomechanics; Brillouin scattering; electrostriction; radiation pressure.

DOI 10.1515/nanoph-2014-0004
Received June 28, 2013; accepted July 18, 2014; previously published online September 30, 2014

***Corresponding author: Alejandro Martínez,** NanophotonicsTechnology Center, Universitat Politècnica de València, Camino de Vera s/n, 46022 Valencia, Spain, e-mail: amartinez@ntc.upv.es
Yan Pennec, Bahram Djafari-Rouhani and Mourad Oudich: Institut d'Electronique, de Microélectronique et Nanotechnologie, UMR CNRS 8520 Université Lille 1, Villeneuve d'Ascq 59653, France
Vincent Laude and Jean Charles Beugnot: Institut FEMTO-ST, Université de Franche Comté, UMR CNRS 6174, Besançon 25044, France
Nikos Papanikolaou: Institute of Advanced Materials, Physicochemical Processes, Nanotechnology and Microsystems, Department of Microelectronics, NCSR "Demokritos" GR-153 10 Athens, Greece
Said El Jallal: Institut d'Electronique, de Microélectronique et Nanotechnologie, UMR CNRS 8520 Université Lille 1, Villeneuve d'Ascq 59653, France; and Physique du Rayonnement et l'Interaction Laser Matière, Université Moulay Ismail, Faculté des sciences, Meknès, Morocco
Jose M. Escalante: NanophotonicsTechnology Center, Universitat Politècnica de València, Camino de Vera s/n, 46022 Valencia, Spain

Edited by Jelena Vuckovic

1 Introduction and basics

Light and sound can propagate through a wide variety of materials in the form of electromagnetic and elastic waves, respectively. From a quantum perspective, both kinds of waves can be described in terms of physical particles: photons for the case of light and phonons for the case of sound. Besides propagating independently from each other, photons and phonons may also interact. The interaction between light and sound, usually called acousto-optic (AO) interaction, has been routinely used for many years in a variety of optical devices to achieve active control of light via elastic waves [1]. Interestingly, when optical and elastic waves are confined at the micro- and nano-scale,[1] their interaction can be strongly enhanced

1 By nanoscale, we refer to structures with sizes below 1 micron.

as a consequence of the increased density of states. As a result, AO interaction in micro- and nano-structures enabled by the advances in nanotechnology has received considerable interest in recent years due to the intriguing effects it can provide [2–17]. For instance, light and sound can strongly interact in cavities supporting both confined photonic and acoustic modes. This is the basic idea behind cavity optomechanics [2–4], which has emerged as an extremely powerful paradigm to couple photons and phonons in unprecedented ways, giving rise to a wide variety of striking phenomena, including laser sideband cooling and optomechanically-induced transparency [7–9]. Besides cavities, light-sound interaction can also take place in properly designed nanoscale waveguides, where such interaction can be enhanced by several orders of magnitude as compared to the effects observed in structures with larger dimensions [15].

Although first attempts to couple light and sound in optical cavities made use of ultra-high Q-factor microspheres [16] or micro-toroids [9], phoxonic [11, 12] or optomechanical (OM) [6] crystals have emerged as an interesting platform to observe all the previous effects at the nanoscale. The main reason is that this approach enables a huge confinement of both kinds of fields down to their corresponding wavelengths size (diffraction limit). In addition, it potentially allows for the integration of thousands of AO components (cavities, waveguides, etc.) on a single chip using mainstream semiconductor fabrication techniques. Phoxonic or OM crystals put together two well-known concepts: photonic [18] and phononic crystals [19, 20]. The main idea behind photonic (phononic) crystals is the introduction of periodicity in the refractive index (acoustic impedance) of a certain propagating medium to get energy intervals for which light (sound) cannot propagate inside the medium: the so-called forbidden bandgaps. We can go a step further and think about introducing periodicity in both the refractive index and the acoustic impedance (for instance, by inserting a periodic array of holes in a slab made of a transparent material) so that bandgaps exist simultaneously for both kinds of waves. The result is a phoxonic crystal: a periodic structure that when properly designed can possess forbidden bandgaps for both light and sound. Phoxonic crystals thus provide a systematic way to engineer point and linear defects that break the periodicity locally and give rise to cavities [21] and waveguides [22] that can ultimately support the confinement and propagation of light and sound waves at certain frequencies within the corresponding bandgaps. It has to be emphasized that these two concepts, OM and phoxonic crystals, are essentially the same: periodic structures that behave simultaneously as photonic and phononic crystals. Throughout this work we will use preferably the term phoxonic crystal.

As a result of wave interference effects, photonic and phononic bandgaps in phoxonic crystals occur at wavelengths of the order of twice the crystal periodicity a. Therefore, photons and phonons controlled by introducing defects in phoxonic crystals have similar wavelengths, which plays a role in what refers to the momentum conservation in an interaction process. However, since light and sound propagation velocities in solids differ by several orders of magnitude, the frequencies of the interacting photons (ω) and phonons (Ω) in cavities and waveguides will be very different. For instance, typical phoxonic crystals displaying a photonic bandgap for infrared photons at about 200 THz (telecom wavelengths), would show a phononic bandgap for phonons with frequencies of several GHz (hypersound) [6, 14]. Since energy (in addition to momentum) is also conserved, more than two particles will be involved in any AO interaction process, being the most typical one the interaction between two photons and one phonon.

In this review we focus on the description of the AO interaction when both optical and elastic (acoustic) waves are localized in small modal volumes (such as nanoscale cavities or waveguides). Our analysis includes the basic mechanisms taking place in OM systems but also attempts a step forward since it includes a full picture of the light-sound interaction at the nanoscale. Notice that OM systems are essentially optical and mechanical oscillators coupled through an AO interaction so that, depending on the coupling strength, the coupled oscillator system could be driven into different regimes [23, 24]). As a result of our analysis, the proposed methods as well as the underlying structures could be used to implement miniaturized AO modulators, to enhance the stimulated Brillouin scattering (SBS) process in waveguides [15], and even to pave the way towards stimulated phonon generation and hybrid photonic-phononic circuits where light and elastic waves are used together to achieve novel functionalities like optical storage [25] or dual sensors.

Since we pay special attention to phoxonic crystals as a systematic way to observe strong light-sound interaction at the nanoscale, we start our review by describing the most suitable structures to get phoxonic bandgaps (Section 2). The different AO interaction processes that can take place in nanoscale structures are described in Section 3. Section 4 shows several examples of AO interactions in nanoscale cavities and waveguides. Finally, some applications resulting from the enhanced AO interaction at the nanoscale are reviewed in Section 5.

2 Phoxonic crystals: periodic structures to manage light and sound at the nanoscale

2.1 Materials for building phoxonic crystals

As a general picture, phoxonic crystals consist of a host medium in which periodic inclusions (typically made by removing the material, for instance, by perforating it with holes) are inserted. The host material has to be transparent for both photons and phonons at the frequencies of interest and has to exhibit high optical/acoustic impedance in order to produce wide bandgaps when the periodicity is inserted. Some employed host materials are silicon (Si) [6], silicon nitride (SiN) [5], indium phosphide [10], aluminum nitride (AlN) [26], and lithium niobate ($LiNbO_3$) [27]. In general, light is produced outside and injected into the phoxonic crystal via optical fibers. In contrast, phonons are created inside the phoxonic structure. In some cases, phonons come from thermal fluctuations which are transduced to the light confined into a high-Q cavity [5]. Phonons can also be created optically by some of the mechanisms discussed in Section 3 (for instance, via radiation pressure). If the host medium displays piezoelectric properties, such as AlN and $LiNbO_3$, hypersound phonons can also be produced via electro-acoustical transducers [28, 29]. This last choice is extremely powerful since it allows for creating photons and phonons independently so that their interaction can be tailored at will. However, and despite some recent attempts [30], the integration of electrically-controlled GHz phonon sources so that acoustic waves can be generated in a controlled and efficient way still remains a formidable technological challenge. Although in the examples below we focus mainly on phoxonic crystal structures built on silicon slabs, all the models explained in this review can be used for all the possible host materials.

2.2 Types of phoxonic crystals

The simplest way to classify phoxonic crystals is according to the number of dimensions for which periodicity occurs. Thus we can have one dimensional (1D), two dimensional (2D) and three dimensional (3D) phoxonic crystals. Only the latter can provide a full 3D phoxonic bandgap, this is, the existence of frequency intervals in which light and sound propagation is completely inhibited no matter the propagation direction we consider. However, 1D and 2D phoxonic crystal structures can also display very interesting features and, importantly, can be much more easily modeled numerically as well as manufactured than their 3D counterparts. As a result, 1D and 2D structures have received most attention so far and we focus mainly on them.

In all the considered structures, the introduction of defects into the otherwise perfect structure can enable the existence of photonic and phononic frequency bands inside the band gap. These modes cannot propagate out of the defect and, as a result, their energy will be localized in the defect region, which can have a transverse size as small as half the wavelength. For instance, we can introduce point defects in order to create phoxonic cavities (in which light and sound can be simultaneously confined) [6, 7], or linear defects to create waveguides with special dispersion properties, e.g., slow photons/phonons [14, 22], not achievable simultaneously in conventional homogeneous materials. Notice that wave confinement in defects can be also achieved without having a full phoxonic bandgap, but partial phoxonic bandgaps for photonic and phononic modes of a given symmetry only, as discussed below. Phoxonic confinement (in the sense of being for both photons and phonons simultaneously) is then effective only for waves respecting this particular symmetry and incident wave fields have to be prepared accordingly. However, fabrication imperfections in a real structure can lead to symmetry breaking, which could result in undesired coupling to modes with other symmetries. The existence of a full phoxonic bandgap would completely avoid such coupling, which could have a strong impact when creating phoxonic cavities and waveguides.

2.3 1D and 2D infinite phoxonic crystals

We start the description of phoxonic crystal structures with the simplest one: a 1D phoxonic crystal, which is formed by an infinite periodic sequence of layers of two (or more) materials having different refractive indices and acoustic impedances, such for instance Si and SiO_2 (see Figure 1A). Since this structure displays translational symmetry with no boundaries in the dimensions perpendicular to the periodic one, propagation is considered to be uniquely along the z-axis, whilst wave vector components along x and y are neglected. Under these conditions, a 1D phoxonic bandgap for modes propagating along z can appear and the insertion of a point defect, as depicted in Figure 1A, can lead to the simultaneous localization of light and sound at certain frequencies [31]. Notice that a very similar 1D structure

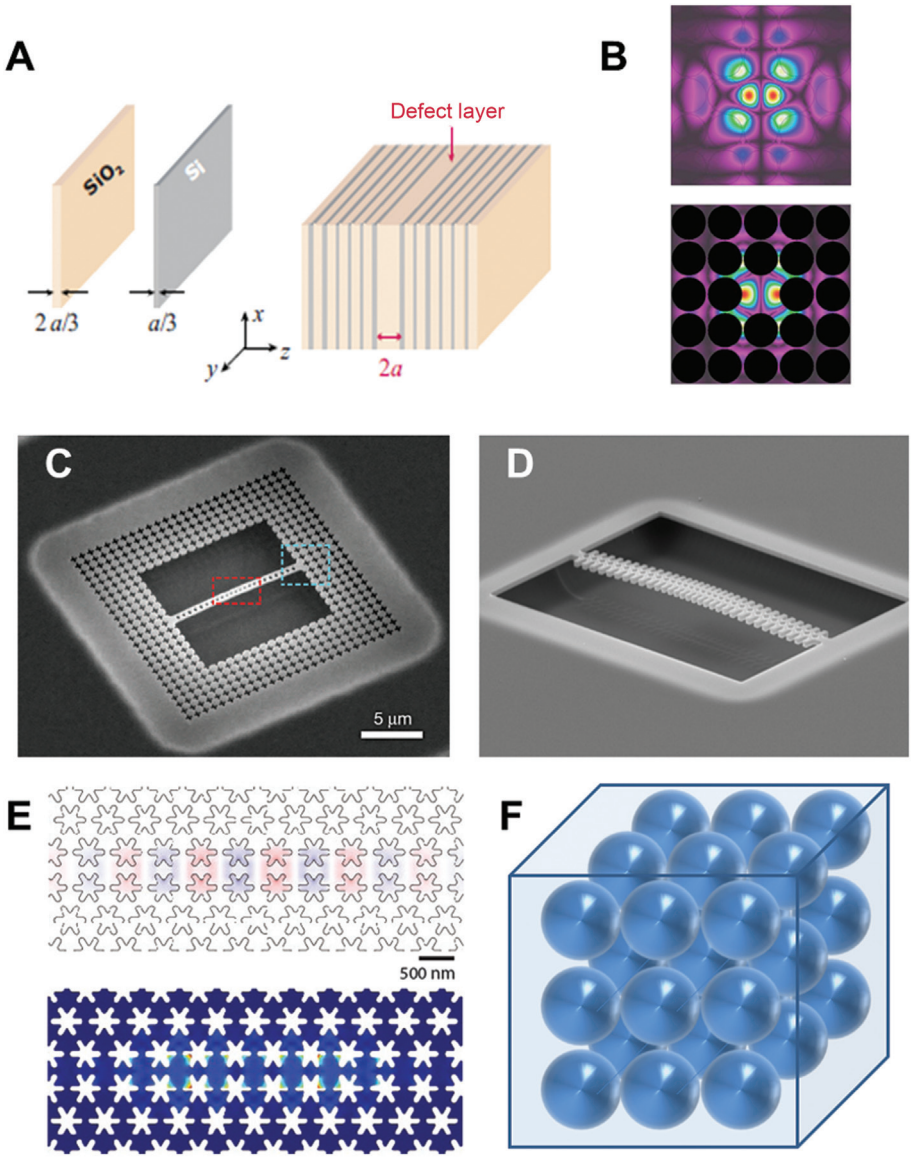

Figure 1 Different phoxonic crystal structures shown in increasing degree of complexity.
(A) A 1D phoxonic crystal is periodic along one dimension (z-axis) by including alternating layers of silicon and silica; a defect layer, created by increasing the thickness of a silica layer up to 2a, *a* being the period, can lead to the localization of light and sound in a certain regions and at certain frequencies (picture from Ref. [31]). (B) Electric (top) and displacement (down) fields in a point defect created in a 2D infinite phoxonic crystal made of silicon perforated by a square lattice of circular holes frequencies (picture from Ref. [21]). (C), (D) Scanning electron images of phoxonic cavities created on two different types of 1D silicon phoxonic crystal slabs. In (C) (picture from Ref. [7]) a series of elliptical holes perforates a silicon strip, which gives rise to partial photonic and phononic bandgaps. A modulation of the ellipses dimensions allows for the creation of a point defect at the middle of the strip. The strip is surrounded by a 2D phononic crystals structure displaying a full phononic bandgap which contributes to reduce mechanical losses. In (D) (picture from Ref. [32]) a series of stubs is added to the array of circular holes in order to provide a full 1D phononic bandgap. (E) Electric (top) and displacement (down) fields at resonance in a point defect created in a 2D "snowflake" phoxonic crystal slab frequencies (picture from Ref. [33]). (F) a 3D array of metallic nanospheres provides a full 3D phoxonic bandgap (Ref. [34]). All figures are reproduced with permission of the different editorials (APS, NPG and AIP).

was first considered by Trigo et al. [35] much before the concept of the phoxonic crystal was proposed. In those experiments, a phononic cavity (super-lattice with periodicity of a few nanometers) was enclosed within two photonic Bragg mirrors forming a Fabry-Perot cavity (a few 100 nm periodicity). THz phonon generation attributed to the strong confinement of both fields was achieved. Because the phononic and photonic periodicities are well different (and also the resulting wavelength of the confined photons and phonons), the structure is not

strictly speaking a phoxonic crystal as we defined before, since different periodicities are considered for localizing phonons and photons. However, it perfectly illustrates the power of the simultaneous confinement and interaction of photons and phonons in nanoscale volumes.

If we add periodicity in another dimension, we get a 2D phoxonic crystal. It was for this geometry that Maldovan et al. introduced the phoxonic crystal concept [21]. Specifically, they considered the case of air holes in silicon as well as the inverse situation, silicon pillars in air. As in the 1D case, the analysis is limited to wave vectors contained in the periodicity plane, so the problem is completely 2D. They found that the first case (holes on silicon) was the most promising, because of the interesting phononic properties of the structure. Figure 1B shows the confined electric and displacement fields at frequencies within the obtained 2D phoxonic band gap obtained when a point defect is inserted in such 2D phoxonic crystal [21]. Clearly, it can be seen the capabilities of such a 2D structure to tightly confine light and sound in a nanoscale volume. Later, Sadat-Saleh et al. [27] performed a comprehensive search of phoxonic band gaps for a 2D infinite crystal of air holes in lithium niobate. This material has a refractive index smaller than silicon, which renders the existence of complete photonic band gaps more difficult; the phononic crystal properties, however, are not strongly affected by the change in the material, because the elastic contrast is given by the free boundaries of the holes, while optical fields extend in the air filling the holes as well as in the matrix.

1D and 2D infinite phoxonic crystals have remained idealized structures not directly accessible to experiments. The reason is that calculations assume an infinite length in the non-periodic dimension as well as wave vectors completely confined in the periodic plane (to avoid closure of the bandgaps), which are conditions difficult to satisfy from a practical point of view. However, for the 2D case, a very close solution is provided by photonic crystal fibers (PCF), which are well known as guides for light with special properties [36]. Interestingly, they can also confine and guide phonons. Unlike in their 2D infinite phoxonic crystal counterparts, propagation of photons and phonons is considered to be along the infinite non-periodic direction, whereas the wave confinement inside the fiber core (which is a linear defect inserted into the 2D periodic pattern) is achieved via the 2D bandgap. Trapped phonons within the solid core of a PCF were predicted and observed experimentally [37]. It was furthermore shown that PCFs can support phononic band gaps and defect-guided acoustic modes can be used to suppress SBS in a silica optical PCF [38].

2.4 1D and 2D phoxonic crystal slabs

A proper way to translate 1D and 2D infinite phoxonic crystals into real structures is to build the periodicity on a slab so that wave confinement in one (for the 2D case) or two (in the 1D case) spatial dimensions is achieved via impedance contrast between the slab material and its surroundings [6]. Such slab structures (see Figure 1C, D and E) were first introduced independently for both photons [39–42] and phonons [43]. For the case of phonons, if the structure is surrounded by vacuum, there is no chance for the phonons to escape from the solid slab. The case is very different for photons. In 1D or 2D photonic crystal slabs, the band gaps should be searched below the light cone, this is, in the frequency-momentum (ω-k) region in which light cannot propagate in free-space. This will ensure the confinement and propagation of the waves along the slab and avoid the radiation of light into vacuum [40]. In contrast, there is no reference to the light cone in infinite 1D or 2D photonic crystals. Notice that here the existence of phoxonic bandgaps is limited to photonic and phononic modes confined in the slab. Such modes can be divided into even and odd parities depending on their symmetry with respect to the plane parallel to the periodicity plane and which divides the slab into two halves. Ideally, 1D and 2D phoxonic crystal slabs should be tailored to display full phoxonic bandgaps, this is, frequency intervals for which the propagation of guided photons and phonons is forbidden for all symmetries. However, this can be quite challenging, although feasible in the 2D case by using square or honeycomb lattice of circular holes perforating a silicon slab (see [12]).

The requirements can be enormously relaxed if we consider the possibility to have partial bandgaps, this is, bandgaps taking place for a given symmetry, as it is typically done in photonic crystals. In a photonic crystal slab, even and odd symmetry modes are completely decoupled so they can be separately excited from the outside by properly choosing the excitation conditions. Defect modes arising in the photonic bandgap when the periodicity is broken will also conserve a given symmetry. Therefore, we can deal separately with each symmetry and try to find partial bandgaps. In real experiments, modes of different symmetries can be accessed just by properly choosing the polarization of the input light (for instance, L3 cavities [41] or W1 waveguides [42] in triangular lattice 2D photonic crystal slabs support even-parity modes which are efficiently excited using TE-polarized light). In principle, the same idea could also be applied to phononic modes, although the practical way to excite separately different symmetries is less obvious. For instance, let us consider

the simplest case: a 1D chain of circular holes in a suspended silicon strip. Such a structure is very well known to support an even parity photonic bandgap which can allocate defect modes in cavities [39]. Concerning its phononic behavior, it does not support a full bandgap for guided modes [43] but a partial bandgap can appear for certain modal symmetries [44]. Using this approach, the localization of photonic and phononic modes with certain symmetries in point defects created on 1D phoxonic crystal slabs possessing partial bandgaps has been recently demonstrated [7, 44].

Unavoidably, fabrication processes will break the physical symmetry of the structure, leading to undesired coupling between modes with opposite symmetries [44]. For the case of point defects, this will mainly result in mechanical losses and a reduction of the mechanical Q-factor of the cavity, which can be a serious drawback in some applications. In Refs. [7, 8, 44], a 1D phoxonic crystal containing a cavity is surrounded by a 2D structure having a full phononic bandgap (see discussions about 2D phoxonic crystals below) to avoid phonon leakage (see Figure 1C). However, this solution does not prevent that some phonons escape from the cavity region by coupling to phonon modes of other symmetries and propagating along the longitudinal direction, which could be prevented if the cavity was created into a 1D phoxonic crystal displaying a full phononic bandgap.

An interesting way to get a complete phononic bandgap in a 1D phoxonic crystal slab is the inclusion of a periodic chain of stubs in addition to the circular holes in a silicon waveguide surrounded by vacuum [45]. The insertion of periodic circular holes in the waveguide is actually sufficient to create a wide photonic band gap for even symmetry modes but the stubbed waveguide adds the full phononic bandgap. The phononic and photonic behavior of this 1D silicon phoxonic crystal slab is described in Section 4.1.3. A cavity inserted in this 1D phoxonic crystal slab would prevent the leakage of phonons out of the cavity in the longitudinal directions, since there are no phononic modes to which phonons scattered in undesired imperfection can couple. The simultaneous localization of light and sound in a cavity created in 1D stubbed phoxonic crystal slab (see Figure 1D) having a full 1D phononic bandgap has been recently demonstrated experimentally [32].

If the slab is perforated by a 2D array of holes, we can get a 2D phoxonic crystal slab. In comparison with the 1D case, the same conclusions regarding the existence of full and partial bandgaps pervade. Point defects can also give rise to cavities for localization of light and sound but in 2D structures we can also introduce linear defects to create phoxonic waveguides (in the sense that they can guide phonons and photons with ideally no losses) [14, 22]. A comprehensive study of the simultaneous existence of absolute phononic/photonic band gaps in silicon slabs perforated by circular holes can be found in Refs. [12, 13]. In [12], the existence of simultaneous phononic and photonic band gaps in finite 2D crystals of various structures constituted by a periodic array of cylindrical holes in a silicon slab, i.e., square, honeycomb, and triangular lattices and, more generally, in centered square and boron nitride lattices, was analyzed. It was found that simultaneous absolute phoxonic band gaps for guided modes can be obtained with the honeycomb lattice. For the square and honeycomb lattices, the simultaneous confinement of both elastic and electromagnetic energy is further possible for certain mode symmetries, this is, partial bandgaps can be found. One can note that the triangular lattice, which is the most widely used in photonic crystal devices, is not appropriate for sound since phononic gaps exist only at very high filling factors. However, the simultaneous localization of light and sound waves in cavities created on a 2D triangular-lattice photonic crystal slab is still possible, although the localization of phonons is caused by impedance mismatching rather than by the existence of a periodic lattice [10]. In the previous cases, the efforts towards obtaining a 2D phoxonic bandgap have been focused on changing the relative dimensions of the periodic cell for a certain lattice but always assuming that there is a single circular hole in it. Wide 2D phoxonic (even-symmetry for photons and full for phonons) bandgaps on dielectric slabs have also be obtained by perforating the dielectric slabs with more complex cross- or snowflake- shaped holes [46]. The co-localization of light and sound waves in a cavity created on a 2D planar snowflake-type phoxonic crystal (see Figure 1E) has been recently demonstrated experimentally [33]. In Section 4.1.2, we will show an example of light and sound localization in cavities created on 2D phoxonic crystal slabs.

For silicon slabs drilled with cylindrical air holes, a complete photonic gap occurs only for a restricted range of the geometrical parameters in the honeycomb and boron nitride lattices, while for a wide range of parameters the phononic gap is accompanied only by a photonic gap with a given symmetry (odd or even) [12]. Instead, in an alternative 2D structure consisting of pillars on top of the silicon plate the complete gaps can exist over a wide range of parameters. In addition, it is not required to choose a relatively high filling fraction, in contrast to the case of air holes in silicon. Using this approach, the existence of 2D phoxonic band gaps has been predicted in a structure constituted by a periodic array of silica pillars deposited on a silicon layer of finite thickness [47].

2.5 3D phoxonic crystals

Absolute phoxonic gaps (in the sense that light and sound propagation is forbidden along all spatial directions for some frequencies) have also been predicted for 3D periodic structures. For example, metallic spheres embedded in an epoxy matrix exhibit phononic band gaps for a wide range of lattices and filling fractions [34]. However, the simulations show that only almost touching spheres in a simple cubic lattice could give absolute phoxonic band gaps. For gold spheres with radius close to half a micron (see Figure 1F), the gaps are predicted at around 1550 nm for light and close to 10 GHz for sound [48]. Similar simultaneous complete phononic and photonic band gaps where also predicted for simple cubic lattices of dielectric spheres connected with dielectric cylinders [49]. Here we should note that by proper engineering of the incoming optical and elastic waves it is also possible to achieve simultaneous localization of the two fields inside partial gaps occurring for certain lattice direction and/or polarization [50].

3 Modeling interaction of light with elastic waves

3.1 AO interaction in nanoscale photonic structures

There are several ways to describe the interaction of photons with phonons inside materials, in either particle or wave terms, or a mixture of both. Let us first give some general physical remarks before proceeding to a description of the different effects we will consider. From a microscopic point of view, photons interact at the atomic scale with the local electronic distribution. The corresponding macroscopic picture is that of the induced dielectric polarization and magnetization of materials in the frame of material Maxwell equations. Similarly, elastic waves satisfy the dynamical equations of continuum mechanics, usually limited to purely elastic contributions for small strains. A microscopic view of the same system leads to the picture of phonons as solutions of lattice dynamics equations. Acoustic phonons, with frequencies well below any internal molecular resonance and with wavelengths much longer than the mean inter-atomic distance, can be understood as being equivalent to continuum elastic waves. It remains that elastic waves or acoustic phonons can both be viewed as collective vibrations of the atomic lattice, with displacements measuring the departure of the centers of mass from their equilibrium positions. The mass of atoms is mostly located in nuclei, but the electronic distribution in the lattice is obviously strongly involved in the exact form of the inter-atomic potentials that enter lattice dynamics equations – or in classical terms, the stiffness or elastic constants of the medium. It is important to remark that the role of electrons is thus essential though indirect in the coupling of optical and elastic waves inside matter.

In the context of structures such as cavities and waveguides, we can concentrate on coherent acoustic phonons in the long wavelength limit and thus treat them as elastic waves. The classical picture of acousto-optics is that a traveling elastic wave will cause a dynamic stress variation inside a material, which will result in a dynamic variation of its refractive index. This so-called photoelastic (PE) effect considered in Section 3.2 is usually described phenomenologically through the material PE tensor [1]. In addition, the travelling acoustic wave causes any material interface it meets to vibrate, for instance the boundaries of a silicon nanophotonic cavity in air. We term the resultant AO modulation effect the moving-interface (MI) effect and discuss it shortly in Section 3.3.

As we just discussed, a propagating elastic wave causes the electronic distribution to be modulated on an acoustic wavelength scale and at acoustic frequencies, and hence the polarization of the medium to oscillate as the elastic wave passes. Reciprocally, volume optical forces are produced along the propagation of optical waves, which act as a driving stress distribution for the generation of elastic waves, the so-called electrostriction (ES) effect described in Section 3.4. In addition, surface optical forces such as radiation pressure can be exerted at the boundaries of a cavity or a waveguide, as we discuss in Section 3.5.

Notice that these different mechanisms can be generally classified into volume and surface effects, depending on whether the AO interaction is manifested in a bulk media or at the interface between two different materials. This idea has been used to schematize the different mechanisms in Figure 2. Moreover, the different effects can also be distinguished depending on the type of wave originating the interaction: PE and MI effects are caused by a propagating acoustic wave that modifies the electromagnetic properties of the host medium whilst ES and radiation pressure induce strain in the material as a consequence of the propagation of an optical wave. The energy exchange between light and elastic vibrations can be seen as a three wave interaction process (see Figure 2). According to this picture, a phonon scatters light inelastically, at another frequency, and creates another photon;

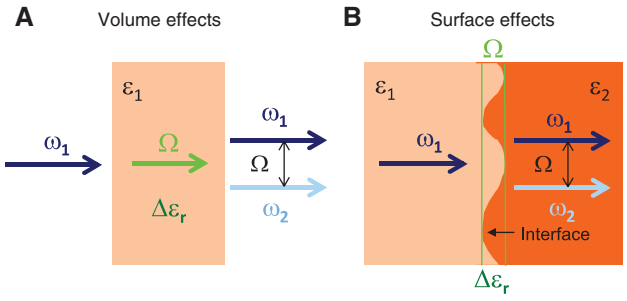

Figure 2 Simplified schemes of (A) volume and (B) surface AO effects. (A) An acoustic wave (frequency Ω) propagating though a bulk medium modifies the permittivity tensor by an amount $\Delta\varepsilon_r$, which affects propagating optical waves (PE effect); A propagating optical wave (frequency ω_1) can also put the medium lattice into vibration, creating an acoustic phonon via ES. (B) An acoustic wave propagates through an interface between two different media and put it into mechanical motion (MI effect), which can affect photons impinging on the interface; Photons impinging on the interface can also put it into motion via radiation pressure. In all the cases, under proper conditions and considering a first-order approximation, a third wave (photon with frequency $\omega_2=\omega_1\pm\Omega$) can result from the coupling between the Ω phonon and the ω_1 photon, such as in the cases of OM coupling in cavities and SBS in waveguides. The different phenomena are described under the framework of three-wave interaction, although in many cases more than three waves can participate in the interaction process.

or the simultaneous propagation of two different light frequencies (two photons) can create an elastic deformation (generate a phonon). However, in many cases, more than three waves can be involved in the interaction process (for instance, two phonons can take part in the scattering process) but always keeping the energy and momentum conservation rules. It should be also highlighted that the strong field overlapping taking place when confining light and sound at the nanoscale usually leads to the coexistence of several of these effects. Overall, the different coupling mechanisms of moving matter with electromagnetic waves can give rise to many interesting phenomena like Brillouin light scattering by acoustic phonons, SBS in waveguides [15], or cavity optomechanics [2, 3]. All these phenomena put acousto-optics at work in the nanoscale level.

3.2 Photo-elastic effect

The *photo-elastic (PE) effect* (see Figure 2A) as considered, e.g., in acousto-optics, is a phenomenological approach well adapted to experiments [51, 52]. By phenomenological we mean that it is given in the form of a constitutive relation that couples the optical wave equation and the elastodynamic equation. Suppose an elastic wave that propagates in a medium, with the components of the vector displacement field u_i written as

$$u_i(\boldsymbol{r},t)=u_i(\boldsymbol{r})\exp(i(\Omega t-\boldsymbol{K}\cdot\boldsymbol{r}))+\text{c.c.} \tag{1}$$

where Ω and $\boldsymbol{K}$ are the angular frequency and the wave vector of the elastic wave, respectively. If the displacements remain small as compared to the wavelength, then according to the Pockels effect it will induce a change in the inverse of the permittivity tensor at optical frequencies that is linear with the strain (first-order or linear approximation):

$$(\Delta\varepsilon_r^{-1})_{ij}=p_{ijkl}u_{k,l} \tag{2}$$

with p_{ijkl} being the rank-4 photo-elastic tensor, resulting in the nonlinear polarization

$$P_i=\varepsilon_0\chi_{ijkl}E_j u_{k,l} \tag{3}$$

with the electric susceptibility

$$\chi_{ijkl}=-(\varepsilon_r)_{im}(\varepsilon_r)_{jn}p_{mnkl}. \tag{4}$$

In the previous expressions, $\boldsymbol{E}$ is the electric field vector, $\boldsymbol{P}$ is the polarization, ε_0 is the electric permittivity of vacuum, and $u_{k,l}$ is the strain tensor (the subscript "l" means derivative with respect to coordinate x_l). Here we will use Einstein's convention of implied summation on repeated indices of tensors. The above formulation is especially useful in locally homogeneous media, i.e., if the elastic and optical properties do not change at the scale of the displacements, while at the same time they can depend on space and time. Indeed, the driven optical wave equation can be taken as

$$\nabla\times(\nabla\times\boldsymbol{E})+\frac{1}{c^2}\frac{\partial^2(\varepsilon_r\boldsymbol{E})}{\partial t^2}=-\mu_0\frac{\partial^2\boldsymbol{P}}{\partial t^2} \tag{5}$$

where the part of the permittivity that is directly influenced by elastic waves, in the right-hand side of the equation, has been purposely separated from the part that does not depend on it, in the left-hand side. The nonlinear polarization $\boldsymbol{P}$ explicitly depends on the phonon frequency as Eqs. (1) and (3) show. In the frame of acousto-optics, where it is generally assumed that the elastic wave is unperturbed by optical waves, the non-linear Eq. (5) can be transformed into a set of coupled linear equations, using an expansion in diffracted optical waves, and solved by matrix algebra [53]. In general, Eq. (5) can be solved using the electromagnetic Green dyadic $\boldsymbol{G}^0(\boldsymbol{r}, t; \boldsymbol{r}', t')$ of the unperturbed system without the AO interaction.

The electric field is given by the Lippmann-Schwinger equation for the electric field component of the wave scattered due to the AO interaction can be written in a Born series [31]:

$$\begin{aligned}\boldsymbol{E}(\boldsymbol{r},t)=\boldsymbol{E}_0(\boldsymbol{r},t)+\frac{1}{c^2}\int d^3r'\int dt'\boldsymbol{G}^0(\boldsymbol{r},t;\boldsymbol{r}',t')\Delta\varepsilon_r(\boldsymbol{r}',t')\partial_{t'}^2\boldsymbol{E}^0(\boldsymbol{r}',t')\\ +\frac{1}{c^4}\int d^3r'\int dt'\int d^3r''\int dt''\boldsymbol{G}^0(\boldsymbol{r},t;\boldsymbol{r}',t')\Delta\varepsilon_r(\boldsymbol{r}',t')\\ \times\partial_{t'}^2\boldsymbol{G}^0(r',t;r'',t'')\Delta\varepsilon_r(\boldsymbol{r}'',t'')\partial_{t''}^2\boldsymbol{E}^0(\boldsymbol{r}'',t'')+\ldots\end{aligned} \tag{6}$$

where $\boldsymbol{E}^0(\boldsymbol{r}, t)$ is the wave field if the AO interaction is ignored, while the time derivative of $\Delta\varepsilon_r$ is neglected. It can be shown that the electric field can be expressed in the following series expansion

$$\boldsymbol{E}(\boldsymbol{r},t)=e^{-i\omega t}\sum\nolimits_{n=0,\pm1,\pm2}\boldsymbol{E}_n(\boldsymbol{r})e^{-in\Omega t}. \tag{7}$$

This means that the total outgoing (transmitted plus reflected) wave consists of an infinite number of monochromatic waves with frequencies ω, $\omega\pm\Omega$, $\omega\pm2\Omega$, ..., which result from elastic and inelastic photon scattering involving absorption and/or emission of zero, one, two, or more phonons. Moreover the intensities of the above series expansion determine the corresponding inelastic light scattering cross sections. In case of small AO effect, the corresponding Fourier spectrum is essentially dominated by the first-order term (three-waves interaction framework) while all higher-order terms are at least one order of magnitude smaller. This is the behavior expected in a usual pump-probe or Brillouin/Raman scattering experiment where single-phonon processes are involved and expansion up to first order is sufficient. This is also the case in most of the theories employed to describe cavity optomechanics phenomena, where a first Born approximation for the AO interaction is used. However, if the optical and acoustic modes are both simultaneously localized with a strong spatial overlap, a very strong interaction is possible and, even for moderate initial elastic strains, more terms are required in the Born-series expansion of the Lippmann-Schwinger equation for an accurate description of the interaction process.

3.3 Moving interface effect

As it travels, an elastic wave deforms the interface between two different materials. Indeed, within a thin layer in the vicinity of the interface with a thickness proportional to the displacement field normal to the interface, the volume originally occupied by material 1 is now occupied by material 2 and vice-versa. Thus, it results in a modification of the dielectric constant that in turn affects the propagation of the optical waves. The *moving interface* (MI) effect will then be proportional to the displacement field and to the difference between the dielectric constants of the materials on both sides of the interface, as schematized in Figure 2B. As mentioned previously, there are five orders of magnitude between elastic frequencies (up to the GHz range) as compared to optical frequencies (a few hundred THz) in typical phoxonic structures. As a result, at any particular instant in time τ the optical wave can be described as seeing a deformed but static medium, described by the spatial distribution of $\varepsilon_r(\boldsymbol{r}, \tau)$ appearing in Eq. (5). By decomposing the period T of the elastic wave in a number of snapshots, the induced effect on optical propagation can then be straightforwardly computed [8]. In a cavity, the shape of the resonator will change over time, and the variation of the resonant frequency of a particular optical cavity mode can readily be obtained as a function of the acoustic strain. In a waveguide, it is similarly possible to consider the variation of the dispersion relation of a particular guided wave as a function of the acoustic strain. It is important to note that unlike the PE effect, which further depends on PE tensor [Eqs. (2–4)], the MI contribution to the AO effect depends only on the refractive indices of the materials on both sides of the interface. Needless to say, it vanishes for equal refractive indices.

3.4 Electrostriction of acoustic phonons

Having discussed the influence of an elastic wave on the modulation of light, we now consider the reciprocal effect of light on elastic waves. The PE tensor couples light with elastic waves, but light can also induce a strain field through *electrostriction* (ES), which is the complementary of the PE effect if we look at the kind of wave launching the interaction. This is described as an optical volume force that drives the elastic wave equation

$$\rho\frac{\partial^2u_i}{\partial t^2}-(c_{ijkl}u_{k,l})_{,j}=T^{es}_{ij,j}, \tag{8}$$

where c_{ijkl} are the elastic tensor components and the ES stress tensor given by

$$T^{es}_{ij}=-\varepsilon_0\chi_{ijkl}E^{(1)}_kE^{(2)*}_l. \tag{9}$$

Both PE and ES effects are for instance involved in the SBS process (see Section 3.7), which is often understood as a single monochromatic optical wave propagating through

a material, and a Stokes wave is backscattered while an acoustic wave is generated, again in a three-waves interaction picture [54]. We will illustrate the ES effect in the case of phoxonic waveguides in Section 4.2.

3.5 Radiation pressure

Radiation pressure is the pressure exerted by incident photons impinging on a surface. Part of the momentum of the incident light is transferred to the surface which is put in motion (see Figure 2B). This way, light can manipulate nano-objects, through the force exerted by radiation pressure [17]. Although the involved forces are extremely small, there are some ways to increase the interaction up to noticeable levels. For instance, this can be done by using photonic cavities: a photon bounces back and forth on the cavity walls many times, so the radiation pressure effects can be enhanced by orders of magnitude [2]. Radiation pressure plays a key role in cavity optomechanics, as it is use to put in motion the mirrors surrounding an optical cavity [3]. The basics of OM coupling taking place in cavities is described in the next section.

3.6 Optomechanical coupling in cavities

Light confinement in micron-sized photonic cavities opened the way towards a platform for controllable transduction between electromagnetic and elastic waves. This coupling of light with the mechanical motion of micro- and nano-resonators has attracted a lot of attention recently, in direct relation with the field of cavity optomechanics [2, 3]. There are many publications describing the OM interaction mainly using a coupled mode theory assuming that the interaction between optical and elastic modes is weak and can be treated with a first order perturbation approach [55, 56]. In brief, tuning a laser at the resonance frequency of an optical cavity will trap light at the cavity region and allow for momentum transfer from light to the material via radiation pressure. Such a deformation will detune the cavity resonance and produce a mechanical vibration through a feedback mechanism which is controlled by the AO interaction. In submicron structures, where the interface to volume ratio is large, the MI effect has also a significant contribution and this allowed the demonstration of OM effects in materials independent of their PE coefficients. In the case of coupled waveguides, Povinelli et al. [57, 58] proposed that the optical gradient force is given by

$$F = -\frac{1}{\omega} g_{\mathrm{OM}} U \tag{10}$$

where U is the total system energy, ω is the eigenmode frequency of the resonant system, and

$$g_{\mathrm{OM}} = \left.\frac{\partial \omega}{\partial x}\right|_{k} \tag{11}$$

is the so-called OM coupling coefficient. This last parameter stands for the variation of the optical resonant frequency when the "relevant" distance in the system varies; for coupled waveguides, this distance is the length of the air gap separating them, while spatial phase matching is achieved. The g_{OM} coefficient is essentially determined by the strength of the AO interaction. The derivation of Eq. (10) involves the idea that a change in internal energy of the coupled system should equal the work done by the mechanical force. This *ad hoc* approach has been practically successful, but gives no clue as to the relation between the optical field generating the force and the detailed vibrations induced inside the resonator (i.e., in contrast with expressions such as Eqs. (8, 9) that dictate the precise elastic wave dynamics). To eliminate possible ambiguities that arise when applying g_{OM} to some systems, a related parameter is typically used [59]: the vacuum OM coupling rate, $\tilde{g}$, is the frequency shift of the photonic resonance when the motion of the resonator has an amplitude equal to the zero-point fluctuation amplitude [7]:

$$\tilde{g} = g_{\mathrm{OM}} \sqrt{\hbar / 2 m_{eff} \Omega} \tag{12}$$

where m_{eff} is the effective mass of the cavity under study. In the context of the optical excitation of the mechanical motion of nanomechanical resonators, the OM coupling defined by Eq. (12) is used to quantify the coupling rate between the optical and the mechanical modes of the resonator [7]. In this picture, its value is an intrinsic characteristic of the resonator, independently of the external optical waveguide that couples photons in and out of the resonator. Since it depends on the field distributions of the optical and mechanical modes, it must be obtained via integration over a volume fully containing the resonator.

Phoxonic cavities with enhanced AO interactions like the ones that we present in this work are perfect candidates for the demonstration of OM coupling, as already demonstrated [6, 7, 32]. However, here we should note that the phenomenological description of OM coupling strength in terms of g_{OM} could become questionable in the strong coupling regime, and a generalization of the coupled mode theory to allow for multiphonon interaction paths is required in this case.

3.7 Stimulated Brillouin scattering in nanoscale waveguides

Another important manifestation of the AO interaction is when two optical modes, with small difference in their frequency, interfere in a background of thermal noise. Then, the two optical waves can be coupled through a phonon provided the three waves conserve momentum and energy. The interference of the two optical waves increases the occupation number of the particular phonon mode through the ES mechanism, which in turn enables stimulated energy transfer between the two optical waves. This picture can be equivalently described as the interaction of two photons and a phonon, as in the Brillouin effect, making the introduction of phase-matching easier [60, 61]. Specifically, we represent the optical wave as the superposition

$$\begin{aligned}\boldsymbol{E}(\boldsymbol{r},t)=&\boldsymbol{E}^{(1)}(\boldsymbol{r})\exp(i(\omega_1 t-\boldsymbol{k}_1\cdot\boldsymbol{r}))\\&+\boldsymbol{E}^{(2)}(\boldsymbol{r})\exp(i(\omega_2 t-\boldsymbol{k}_2\cdot\boldsymbol{r}))+c.c.\end{aligned}\tag{13}$$

Phase-matching in the three-wave interaction is strictly achieved if $\Omega=\omega_1-\omega_2$ and $\boldsymbol{K}=\boldsymbol{k}_1-\boldsymbol{k}_2$. Equation (13) then leads to

$$(\nabla\times(\nabla\times\boldsymbol{E}^{(2)}))_i+\frac{\omega_2^2}{c^2}\varepsilon_r E_i^{(2)}=-\frac{(\omega_1-\Omega)^2}{c^2}\chi_{ijkl}E_j^{(1)}u_{k,l}^*\tag{14}$$

and

$$(\nabla\times(\nabla\times\boldsymbol{E}^{(1)}))_i+\frac{\omega_1^2}{c^2}\varepsilon_r E_i^{(1)}=-\frac{(\omega_2+\Omega)^2}{c^2}\chi_{ijkl}E_j^{(2)}u_{k,l}.\tag{15}$$

Remarkably, the ES process induces an optical volume force that drives the elastic wave equation according to [7]:

$$\rho\frac{\partial^2 u_i}{\partial t^2}-(c_{ijkl}u_{k,l})_{,j}=T_{ij,j}^{es}\tag{16}$$

with the ES stress tensor given by

$$T_{ij}^{es}=-\varepsilon_0\chi_{ijkl}E_k^{(1)}E_l^{(2)*}.\tag{17}$$

Equations (16) and (17) are the same as (8) and (9) and are repeated here for convenience. It is important to remark that the same PE tensor enters the non-linear polarization of Eq. (3) and the ES stress tensor of Eq. (16). Actually, it is possible to consider an interaction Hamiltonian for the three-wave interaction so that the dynamical equations (14–16) can be derived from a single energy balance identity [62]. The possibility of energy transfer between a pump wave and signal optical wave mediated by an acoustic wave is especially interesting in the case of guided wave propagation, such as SBS in optical fibers [63]. The same formalism applies equally to other guided wave situations, such as photonic wires [15] or phoxonic crystal waveguides, which would present the additional advantages of stronger field confinement and, ultimately, slow-wave behavior. It is also important to remark that the optical force is the divergence of the electrostriction stress tensor, i.e., $(F_{ES})_i=T_{ij,j}^{es}$. Because of the involved spatial derivative, it is expected that the optical force will be stronger for tightly confined optical fields, but also in case that $|\boldsymbol{k}_1-\boldsymbol{k}_2|$ is large; this is exactly the situation found with SBS. Moreover, it is clear that the modulation induced by the MI effect scales with the displacement of the boundaries, whereas the modulation induced by the PE effect scales with the strain inside the medium. This suggests a cross-over between the two effects depending on the dimensions of the cross-section of the waveguide, as it was found by Rakich et al. for nanoscale rectangular waveguides [15].

4 Light-sound interaction at the nanoscale

4.1 Light-sound interaction in cavities

In this section, we show how the AO interaction between light and sound can be modeled in cavities created on finite or infinite 1D and 2D periodic structures. Although we have chosen silicon as the host material, our analysis here is quite general and could be applied to other materials as well as to other kinds of phoxonic structures. The cavities consist of point defects properly chosen so that photonic and phononic modes with frequencies within the bandgap region appear to be confined in the defect region. Since the volume occupied by both kinds of modes is of the order of a cubic wavelength, the interaction between photons and phonons can be very strong, mostly if the cavities are designed to have very high Q factors (very large lifetimes of photons and phonons in the defect region).

4.1.1 Cavity in a 2D infinite phoxonic crystal

It is expected that the high level of energy confinement in phoxonic crystal cavities enhances both PE and MI couplings. As reported in Section 3, an acoustic wave induces

a variation of the refractive index due to the elastic strain and the confinement of elastic energy leads to a strengthened index variation. In addition, when the electromagnetic energy is trapped in a high Q factor cavity, the mechanical displacement of the cavity boundaries induces a modulation of the resonant frequency of the optical cavity [56]. To illustrate this idea, we consider a cavity created by a point defect in an infinite 2D phoxonic crystal consisting in a square lattice (period a) of holes of radius r/a=0.48 on silicon [11]. Our goal is to investigate the modulation of optical modes of the cavity through the PE (volume) and MI (surface) effects. The results presented below are computed using the finite element method (FEM). However, we remark that other methods could be used to calculate the optical and acoustical fields prior to the calculation of the interaction parameters.

The cavity is defined by filling one hole in the perfect structure. The phononic band structure is calculated considering a super-cell constituted of the cavity surrounded by seven unit cells on each side. The separation between two neighboring cavities is chosen to be sufficiently large to avoid interaction between them. Figure 3 shows the modal profiles of the phononic modes and of the TM polarized photonic modes inside the phoxonic bandgap. In our calculations, TM (TE) polarization signifies that the magnetic (electric) field is along the z-axis. TE modes are not considered here as they display a lower confinement than TM modes. Cavity modes are labeled in ascending order using letters for phononic modes and lowercase Greek letters for TM optical modes. In Figure 3 as well as in the rest of this section, reduced acoustic frequencies are given in dimensionless units ($\Omega a/2\pi c_t$), where c_t is the transverse velocity of sound in silicon for the crystallographic direction [100] (c_t=5844 m/s), whilst normalized photonic frequencies are given in dimensionless units a/λ, where λ is the wavelength of light in vacuum. For this particular case, if the lattice constant is a=760 nm, the TM photonic bandgap occurs at wavelengths around 1550 nm (telecom

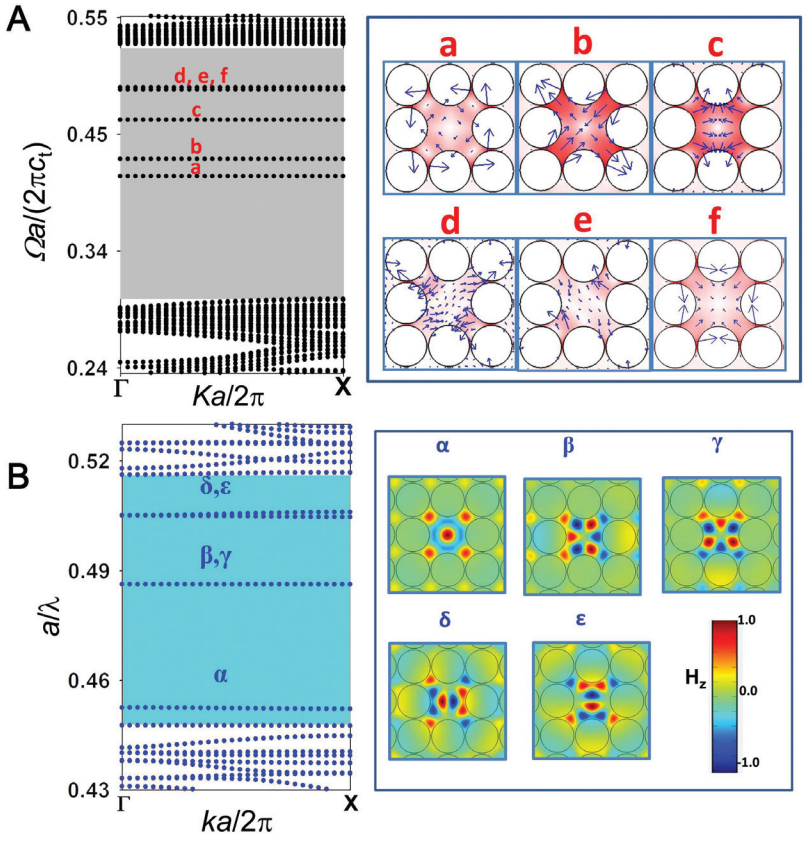

Figure 3 Photonic and phononic localization in a cavity in a 2D infinite phoxonic crystal consisting of a square-lattice of circular holes in a silicon matrix.

(A) Eigenfrequencies of the six phononic cavity modes and corresponding displacement fields. The phononic bandgap is highlighted in gray color. For each cavity mode, the blue arrows indicate the displacement field vector $\boldsymbol{u}=(u_x,u_y)$ for some spatial positions. (B) Eigenfrequencies of the TM optical cavity modes (left) and corresponding magnetic field distributions (right). The photonic bandgap for TM polarization is highlighted in blue.

window), while the phononic bandgap will then occur at acoustic frequencies between 2.34 and 4.04 GHz.

In Figure 3A, one can see that six modes are located in the phononic bandgap. As seen from the displacement field distributions, the main deformations are essentially localized inside or in the close vicinity of the cavity. For instance, mode 'a' is essentially a shear mode causing the cavity to twist back and forth during an acoustic period. The time evolution of mode 'b' results in a deformation of the cavity in such a way that one diagonal stretches while the other contracts during half an acoustic period. During each half acoustic period, the mode labeled 'c' alternatively expands along one of its sides and contracts along the other sides. Modes 'd' and 'e' are degenerate and their distribution profiles are mutually orthogonal. Finally, the mode labeled 'f' is essentially a breathing mode causing only slight distortions of the cavity shape. Figure 3B shows that five optical cavity modes with TM polarization appear inside the photonic band gap. The first mode α is followed by two pairs of degenerate modes: β and γ; and δ and ε.

As described in Section 3, two coexisting mechanisms involving local variations of the dielectric permittivity are responsible of the AO interaction: the PE and the MI effects. In a cavity, the former effect is due to the acoustic strain distribution via the Pockels effect whereas the latter effect takes into account the dynamic motion of the silicon-vacuum boundaries at the holes. Numerically, we have considered two methods for the calculation of the AO interaction. The first one is based on a quasi-static approximation which is justified by the fact that the optical frequency ω is by five orders of magnitude higher than the acoustic frequency Ω. In other words, the calculation of optical cavity modes can be performed at several selected times within an acoustic period, with the phononic mode profile considered frozen. The second method consists in calculating the so-called OM coupling coefficient as introduced in Section 3 and summarized by Chan et al. [44]. The general expression for the coupling coefficient given by Eq. (11) is developed here for the case of cavities. First, the contribution of the MI effect is given by

$$g_{\mathrm{OM,MI}} = -\frac{\omega}{2}\frac{\oint_{\partial\upsilon}(\mathbf{Q}\cdot\mathbf{n})(\Delta\varepsilon|\mathbf{E}_{\parallel}|^2 - \Delta\varepsilon^{-1}|\mathbf{D}_{\perp}|^2)\mathrm{dS}}{\int_{\mathrm{V}}\mathbf{E}^{*}\cdot\mathbf{D}\mathrm{dV}} \qquad (18)$$

where $\mathbf{Q}$ is the normalized displacement field (with $\max|\mathbf{Q}|=1$), $\mathbf{n}$ is the outward facing surface normal, $\mathbf{E}$ is the electric field, $\mathbf{D}$ is the displacement field, subscripts // and $\perp$ indicate field components parallel or perpendicular to the surface, respectively, ε is the material permittivity, $\Delta\varepsilon=\varepsilon-\varepsilon_{\mathrm{air}}$, and $\Delta\varepsilon^{-1}=\varepsilon^{-1}-\varepsilon_{\mathrm{air}}^{-1}$. Second, the PE contribution is derived from first-order perturbation theory as

$$g_{\mathrm{OM,PE}} = -\frac{\omega}{2}\frac{\langle\mathbf{E}|\delta\varepsilon|\mathbf{E}\rangle}{\int_{\mathrm{V}}\mathbf{E}^{*}\cdot\mathbf{D}\mathrm{dV}} \qquad (19)$$

So, in Eqs. (18) and (19), $g_{\mathrm{OM,MI}}$ and $g_{\mathrm{OM,PE}}$ correspond to the MI and PE contributions of the OM coupling coefficient defined by Eq. (11). An analysis of the symmetry can be done to discriminate the phonon-photon mode pairs that provide a vanishing AO coupling. We consider the first order of the acoustic deformation (one phonon exchange) and search for the phononic/photonic pairs for which the OM interaction can take place. If the photonic mode is non-degenerate, Eqs. (18) and (19) show that, whatever the symmetry of the photonic mode, the coupling coefficients vanish if the acoustic mode displays an even-even (ee) symmetry with respect to both vertical and horizontal symmetry planes of the cavity. Among the six phononic modes shown in Figure 3A, only (c) and (f) have this property. If two photonic modes are degenerate, they can display a finite coupling even for a phononic mode with ee symmetry. This is because the coupling coefficients should be written as a matrix where the non-diagonal elements can be different from zero. The key roles played in AO coupling by mode symmetry and degeneracy are discussed more in depth in Ref. [64].

As an illustration, the AO interaction is further analyzed for phononic modes '*b*' and '*f*' with the nondegenerate photonic mode α and the doubly degenerate modes β and γ. Indeed, these cases provide the strongest AO couplings and furthermore cover the main variety of situations that can be met. We calculated the modulation of the TM optical modes during one acoustic period ($0<\Omega t<2\pi$). The results are depicted in Figure 4. This approach allows to compare the relative magnitude and sign of the PE and MI effects for each phonon-photon pair. For the sake of computational facilities, these results are presented when the amplitude of the acoustic vibrations is such that the maximum displacement in the cavity is 1% (10^{-2}). Actually, this deformation is much greater than more realistic values of 10^{-4} to 10^{-6} even if the acoustic excitation was generated by an acoustic source. However, for the phononic mode f where the modulations of the optical modes versus time display a sinusoidal behavior (see Figure 4 and discussion below), we have checked that the optical modulations remain proportional to the vibration amplitude, so they are scalable. For the phononic mode b, the bigger acoustic amplitude allows to see the effect of non-linearities, namely the exchange of more than one phonon during the interaction process when the acoustic strain is sufficiently strong.

We notice that phononic modes 'b' and 'f' have qualitatively different effects on the photonic modes. The breathing phononic mode 'f' produces an almost

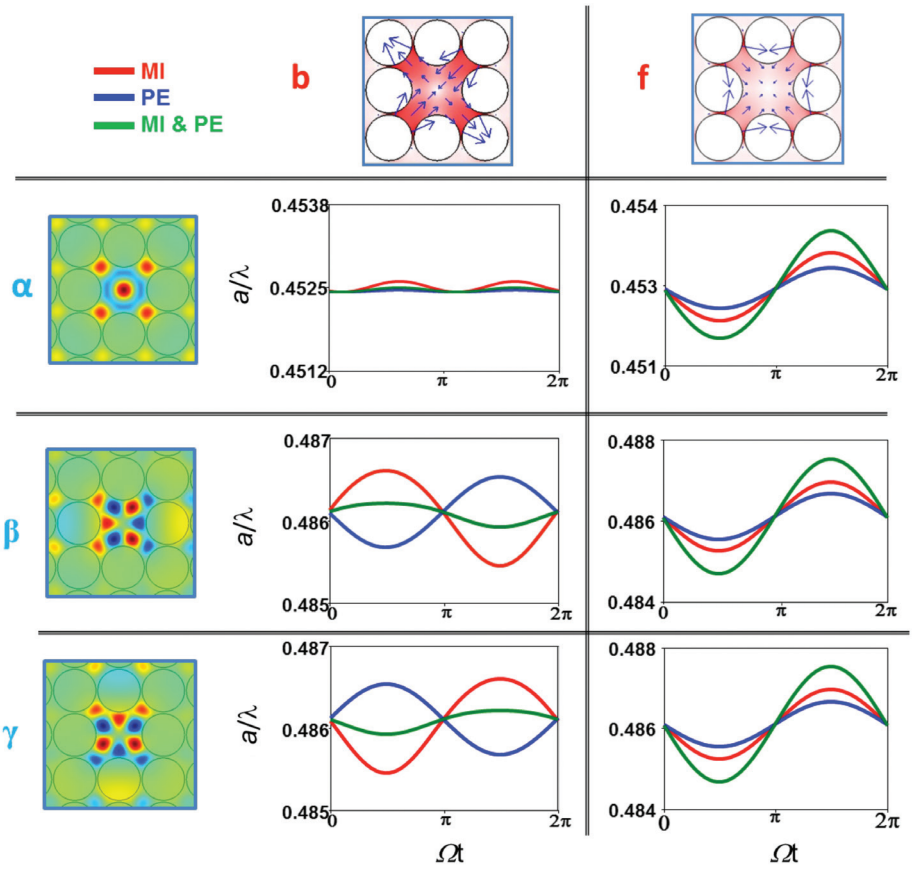

Figure 4 AO interaction in the cavity described in Figure 3. Modulations of the TM photonic modes α (upper panels), β and γ (lower panels) induced by the phononic modes 'b' and 'f'. The graphs present the photonic frequency variation as a function of Ωt during one period of the phononic mode. Green-solid curves represent the full results when both interaction mechanisms are taken into consideration while red and blue lines are drawn respectively for MI and PE effects acting alone.

sinusoidal modulation of each of the photonic modes and does not lift degeneracy. In contrast, the frequency modulation of photonic mode α by phononic mode 'b' resembles the square of a sinusoidal function. This modulation contains a Fourier component at 2Ω, which means an AO interaction with two-phonon exchanges, so more than three-waves take part in the interaction process. The evolution of modes β and γ displays the shape of a slightly distorted sinusoidal function and their degeneracy is lifted.

Comparing the strength of both AO mechanisms PE and MI contributions, one can notice that the MI contribution is dominant in all cases considered here, although both contributions are of the same order of magnitude. Obviously, when the amplitudes of both contributions are added, their relative phase must be taken into account. When the cavity is perturbed by phononic mode 'f', the two contributions are in phase. In contrast, the two contributions are out of phase for the pairs (b, β–γ). Finally, in the case of the pair (b, α), the PE contribution is almost negligible. We conclude that in order to maximize the AO interaction, it is of paramount importance to design the phoxonic cavity so that both contributions, PE and MI, not only have high amplitude but exhibit also the same phase so they add coherently. Moreover, the PE contribution to the AO interaction can be increased especially owing to the significant variation of the PE coefficients that occurs near a semiconductor band gap. This point was discussed recently for silicon and gallium arsenide crystals [64].

4.1.2 Cavity in a 2D phoxonic crystal slab

Similarly to the 2D infinite case, the interaction between phonons and photons inside a cavity can be investigated in a silicon slab drilled with air holes organized in a square lattice [65]. For definiteness, the phoxonic crystal was chosen with the geometrical parameters a=540 nm, h=325 nm and r=215 nm. According to Ref. [12], this set of parameters results in an absolute phononic band gap in the frequency range [5.86, 6.02 GHz] and a photonic gap

of even symmetry in the wavelength range [1455, 1610 nm]. The cavity is now defined by removing three holes inside the perfect structure, as shown in Figure 5. This cavity, which can be named as L3 since it is built by removing three holes as in the typical L3 cavity in triangular-lattice photonic crystal slabs [41], leads to four phononic cavity modes inside the absolute phononic band gap and to three photonic modes inside the photonic gap of even symmetry. In Figure 5, the elastic and the electromagnetic field distributions are presented for the phononic mode at 5.95 GHz and the three photonic modes at 1571 nm, 1515 nm, and 1476 nm. It can be seen that all modes are well confined inside the cavity, and that the spatial extension of the fields is of the order of the wavelength. The AO coupling between the phononic mode and the three photonic modes was calculated considering the two coexisting mechanisms, the PE and the MI effects, as before. As above, the maximum displacement in the cavity is 1% and the modulation of the three photonic modes during half an acoustic period is calculated and represented for each effect separately. One can notice a significant sinusoidal modulation of each photonic mode by the acoustic mode. Nevertheless, the origin of the modulation is different for each photonic mode. For the first mode, the coupling is mainly due to PE effect, for the second it is due to both PE and MI effects, and for the third mode it is due to the MI effect. The calculated OM coupling rates are also shown in Figure 5 for each mode. Their values show coherent relative motion with the coupling strengths derived directly from the temporal modulation of cavity photonic modes. In comparison, however, the numerical evaluation of coupling rates is significantly faster. While the coupling rate found for the L3 cavity remains relatively low (1 MHz at maximum), we have found coupling rates up to 2.47 MHz for another type of defect, detailed in Ref. [64] and named cross cavity (consisting mainly in two intersecting L3 cavities), which are slightly larger than the values found in the literature for similar slab structures.

4.1.3 Cavity in a 1D phoxonic crystal slab

The same approach can also be applied to 1D phoxonic crystal slab cavities. Specifically, we consider a point defect created on the 1D stubbed silicon waveguide perforated by holes as described in Figure 6. The structure possesses two symmetry planes, Π_y (normal to the y-axis) and Π_x (normal to the x-axis). It can be shown that, keeping geometrical parameters of the stubs that are suitable for the opening of the phononic band gap, an increase in the diameter of the holes leads to a variation of the photonic dispersion branches [45]. Although there is no absolute photonic band, one can find many partial band gaps for specific symmetries with respect to symmetry planes. Now, if the period a is chosen to be 500 nm, and all the other geometrical parameters as reported in the caption of Figure 6, the structure presents a full phononic band gap in the frequency range [3.54, 4.11 GHz] and a partial photonic band gap in the telecom range [1350, 1612 nm]. The

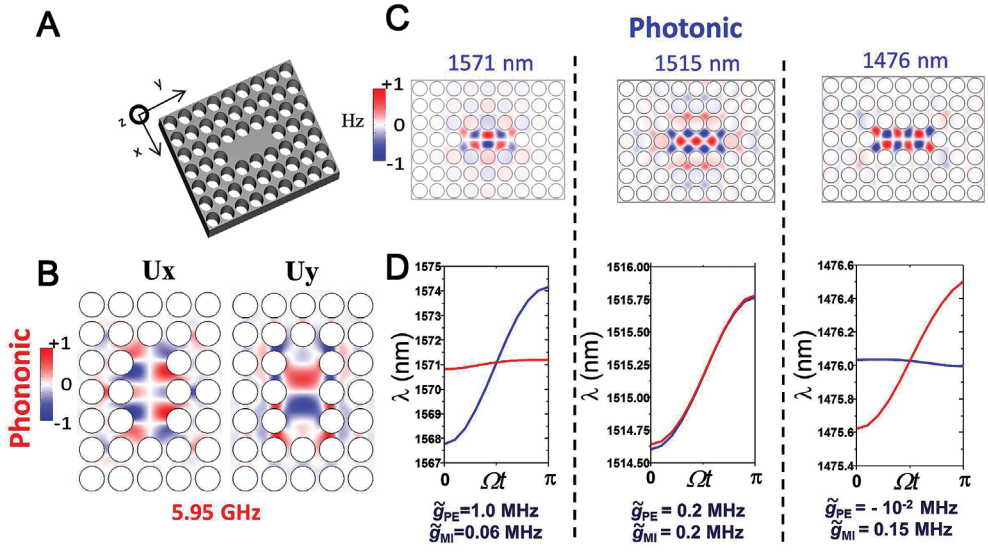

Figure 5 Light-sound interaction inside an L3 cavity in a 2D square-lattice silicon phoxonic crystal slab.
(A) 3D schematic view of an L3 cavity inside the square-lattice periodic silicon slab. Field maps: Representation of (B) one phononic (5.95 GHz) and (C) three photonic (1571 nm, 1515 nm and 1476 nm) eigenmodes of the L3 cavity (C). (D) Modulations of the three photonic modes frequencies induced by the phononic mode during half period and the corresponding coupling rates. The blue (red) curves represent the PE (MI) contribution.

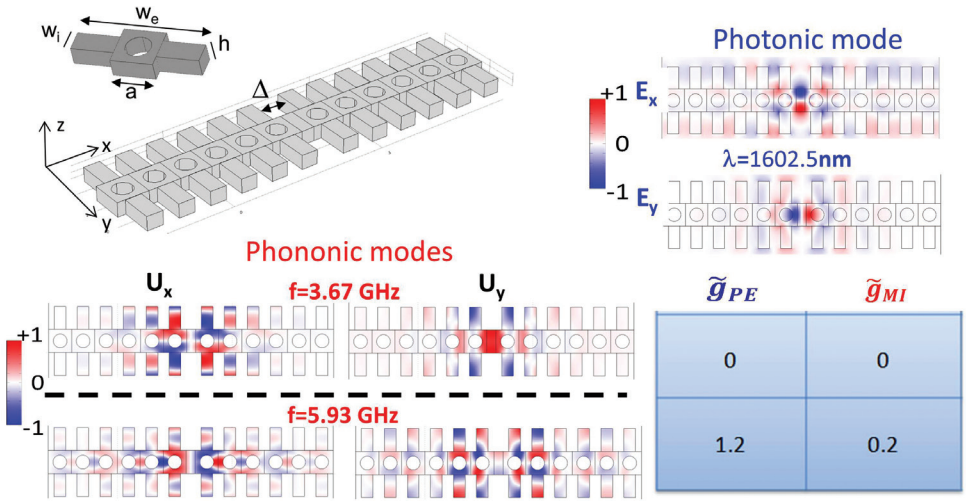

Figure 6 Schematic view of the elementary unit cell that is used in the calculations and the cavity defined by the length Δ created inside a 1D silicon phoxonic crystal. Components of elastic (GHz) and magnetic (nm) fields of phononic and photonic eigenmodes for a cavity of length Δ=200 nm. Numerical values of the PE and MI coupling rates are given in the table. The geometrical parameters are: w_e/a=3.0, w_i/a=0.5, h/a=0.44, and r/a=0.3 (h is the silicon slab thickness, w_e and w_i are the length and the width of the symmetric stubs, and d=2r is the diameter of the air holes), with a=500 nm.

cavity is created by simply changing the distance between two neighboring unit cells, as depicted in Figure 6. The width of the cavity is characterized by the elongation parameter Δ, i.e., Δ=0 when the crystal is defect-less. The insertion of a cavity of length Δ=200 nm introduces three phononic modes and one photonic mode (at 1602.5 nm), as shown in Figure 6. Unfortunately, the symmetry of all phononic modes in the complete band gap is such that they cannot couple to the photonic mode, and so the AO coupling rates are close to zero, as shown in the first row of the table in Figure 6 for the phononic mode at 3.67 GHz. This leads to conclude that the existence of a phoxonic bandgap is not the only condition to ensure strong AO interaction inside a phoxonic cavity: a significant overlap between photonic and phononic modes must be ensured. However, a high AO coupling is obtained for other phononic modes that fall inside partial band gaps. One example is given in Figure 6 for a phononic mode of even-even symmetry with respect to the planes Π_x and Π_y, which appears at 5.93 GHz. This mode provides high values for both $\tilde{g}_{PE}$ and $\tilde{g}_{MI}$, which, moreover, add in phase. The coupling strength is of the order of other values reported in the literature (for instance, the cavity in Ref. [7]). A phoxonic cavity can also be introduced by periodically changing the structural parameters of the unit cell depicted in Figure 6, which would allow for a higher optical Q factor of the confined modes. Using such approach, the simultaneous confinement of photonic and acoustic modes in a phoxonic bandgap has been demonstrated experimentally [32].

4.1.4 Cavity in a 1D infinite phoxonic crystal

Light-sound interaction can be also studied in the 1D phoxonic cavity shown in Figure 1A, which can be considered the simplest phoxonic structure. Such a study is especially useful since it provides a direct insight on the AO interaction when both optical and elastic resonances are in the same volume. Interestingly, in such a system, the AO interaction can be easily treated correctly beyond the first order Born approximation, as usually done in cavity optomechanics, if we consider the time evolution of the optical wave during one period of the elastic wave. To illustrate this, we consider a phoxonic cavity consisting of a single silica layer sandwiched between two Bragg mirrors, composed of five periods of [SiO_2($2a/3$)-Si($a/3$)] bilayers on the left and right (see Figure 1A), which supports optical and elastic modes localized inside the 1D phoxonic bandgap (see further details in Ref. [31]). Here we present typical results for the photonic transmission spectrum (initially neglecting the AO interaction) for a cavity with thickness a and normally incident light (Figure 7B) together with the transmission spectrum for longitudinal elastic waves propagating normal to the material interfaces (Figure 7A) [31]. The multilayer supports a dual gap for both light and elastic waves, as well as resonances inside the corresponding gaps (Figure 7C and D). To account for the continuous variation of the refractive index in the calculation, we subdivide each layer in a large number of (homogeneous) elementary sub-layers. When the acoustic excitation is switched on, the optical transmission spectrum varies periodically in time with the

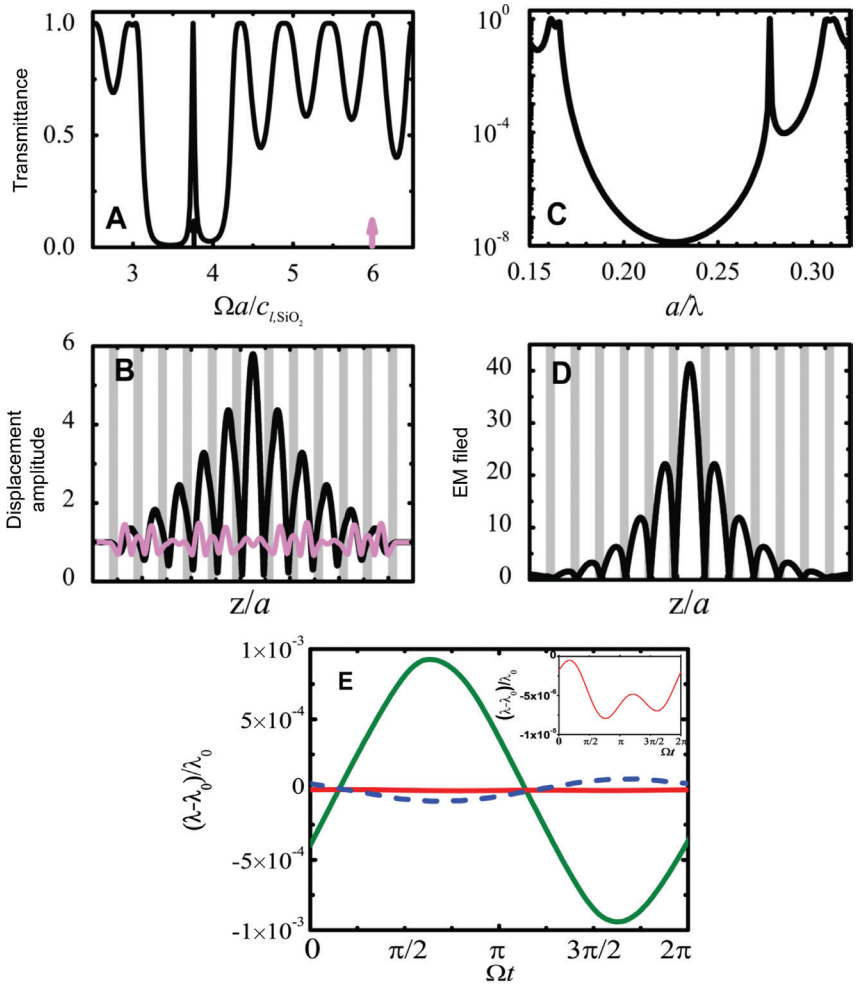

Figure 7 Optical and acoustic wave confinement in a cavity created in the 1D multilayer structure depicted in Figure 1A: two SiO_2/Si Bragg mirrors with lattice constant a separated with a SiO_2 layer of width a.
(A) Elastic transmittance spectrum for a longitudinal wave normally incident on the multilayer structure together with the displacement field shown in (B) for two frequencies, on and off resonance indicated with the arrows in the transmittance spectrum. (C) Optical transmittance spectrum of the same structure for light incident normal to the interfaces. (D) Electromagnetic field profile at the resonance frequency shown in (C). (E) Variation of the optical resonance wavelength (λ_0) with time during a period of the elastic wave. Red line: cavity structure with a SiO_2 layer of thickness a between two Bragg mirrors, and elastic wave on resonance, a zoom of this curve is shown in the inset. Green line: cavity structure with a SiO_2 layer of thickness $2a$ between two Bragg mirrors, and elastic wave on resonance [31]. Dashed blue line: off resonance elastic wave in the case of a $2a$-thick SiO_2 layer.

period of the acoustic wave. In Figure 7E we compare the temporal variation of the optical resonance frequency for two multilayer cavity structures that differ only on the thickness of the central SiO_2 layer placed between the identical Bragg mirrors. The cavity with a $2a$ thick SiO_2 layer shows enhanced AO interaction as reported previously [31], but reducing the SiO_2 thickness to a, results in a strain field $S(z)$ which changes its sign as we cross the middle of the structure (antisymmetric), giving a zero overlap integral with the optical field. In this case, the AO interaction is even smaller than the one expected for an off-resonance elastic frequency (assuming the same input strain level of 10^{-3} in all the cases). To gain more insight it is useful to consider the Fourier transform of the temporal variation of the electric field during one period of the elastic wave. The analysis of the Fourier coefficients in the series expansion of the electric field [Eq. (6)] shows that an enhanced, resonant, AO interaction will scatter light at frequencies ω, $\omega\pm\Omega$, $\omega\pm2\Omega$, $\omega\pm3\Omega$ etc. The first term of the Born series expansion of Eq. (6), gives the intensity of light scattered at $\omega\pm\Omega$ due to

single phonon absorption-emission processes. This is determined by the overlap integral between the optical mode and the strain field of the elastic mode:

$$E_1 \propto \int dz\, p_{12}(z)\varepsilon^2(z)S(z)(E^0(z))^2 + \sum_{z_n}(\varepsilon_{n+1}-\varepsilon_n)u(z_n)(E^0(z_n))^2 \quad (20)$$

where ε is the dielectric permittivity at each position along the stacking direction z, S is the strain and p_{12} is the appropriate AO coefficient. The second term gives the MI contribution. From Eq. (20) we can easily understand that elastic modes with antisymmetric strain field with respect to the center of the cavity will give a zero overlap integral [first term in Eq. (20)] so such elastic modes prohibit single phonon absorption or emission processes. This leads to an overall suppression of the AO interaction, despite the fact that higher order processes involving more phonons could occur. Moreover, in such a case, as shown in the inset of Figure 7E, the cavity frequency shifts only to lower wavelengths. This analysis is appropriate also for the results presented in Figure 4 for the optical mode α and elastic mode b. For layers with submicron thicknesses the frequency of the optical resonance is a few hundred THz, while elastic waves of few GHz are required, just as in the cavities considered before. Such high frequency vibrations experience significant damping that should be carefully considered. Recent studies indicate that multiphonon AO interaction could survive and be observable in multilayer structures [66] even in the presence of realistic material losses.

Multilayer phoxonic cavities have been also considered for modulation of light emission via AO interaction [67]. The enhanced light extraction achieved by placing emitters inside optical cavities can be combined with efficient modulation through a resonating elastic wave. Additionally, single dielectric particles can be also considered as ideal phoxonic cavities, but as the size of the particles is reduced to few microns, excitation of the proper elastic wave is more challenging [68].

4.2 Light-sound interaction in waveguides

In addition to cavities, nanoscale waveguides have also attracted attention recently in view of obtaining simultaneous confinement of propagating elastic and optical waves, and hence potentially strong AO interactions. The main difference with cavities is that in guides waves are allowed to travel along one direction, while transverse confinement results from structuration along the other two directions. The two basic contributions to AO coupling discussed previously, PE and MI, are still at stake, but in addition optical forces are induced in nanoscale waveguides, as exemplified by Brillouin scattering effects [15, 69, 70]. It has been predicted that photon and phonon confinement in a transversal dimension of the order of half the wavelength in nanoscale waveguides of mm-length has the potential to induce a giant Brillouin gain that could be equivalent to km-long silica fibers [71–74]. Both ES (volume) and optical surface forces such as radiation pressure (see Figure 2) were predicted to scale to very large values in nanoscale waveguides [15]. However, the technological challenge of obtaining a free-standing nanoscale waveguide with a length of a few mm or more is very demanding. In practice, it should be connected to a supporting substrate and the anchors will most probably introduce acoustic losses, especially at GHz frequencies. Phoxonic crystal slab waveguides, created by inserting linear defects into 2D phoxonic crystals, should provide an alternative design where simultaneous guidance of photons and phonons inside a nanoscale solid core can be obtained, while the solid core is supported by the holey structure surrounding it. We note here that photonic (and hence phoxonic) crystal waveguides bear similarities with PCFs. In PCFs, however, the periodic structuration runs along the core axis and absolute band gaps are thus not generally obtained.

Phoxonic crystal slab waveguides have the potential to combine the confinement of PCF and nanoscale waveguides with slow-wave propagation. Slow light is at present a very active research field with important applications to enhanced optical nonlinear effects [75]. For the same reason, joint slow sound and slow light propagation holds promises for enhanced AO interactions, as in any other kind of nonlinear interaction [76]. As a first step in this direction, some theoretical studies recently shown that photons and acoustic phonons can be simultaneously guided and slowed down in specially tailored nanostructures (such as 2D phoxonic crystal slab waveguides), by relying on the phoxonic band gap effect [14, 22, 77]. However, an experimental demonstration of such slow-wave-induced enhancement has not been reported so far. In the following, we discuss in some detail the approach followed in [14] and connect it with the ES of acoustic phonons from photons.

The phoxonic waveguide depicted in Figure 8A and B was designed by introducing a linear defect in a 2D phoxonic crystal slab perforated by a square lattice of holes. The parameters of the structure were chosen in order to provide an even-parity 2D photonic bandgap and a full phononic bandgap. The goal of the waveguide design was to obtain a simultaneous spatial confinement of both phonons and photons, provided by the phoxonic

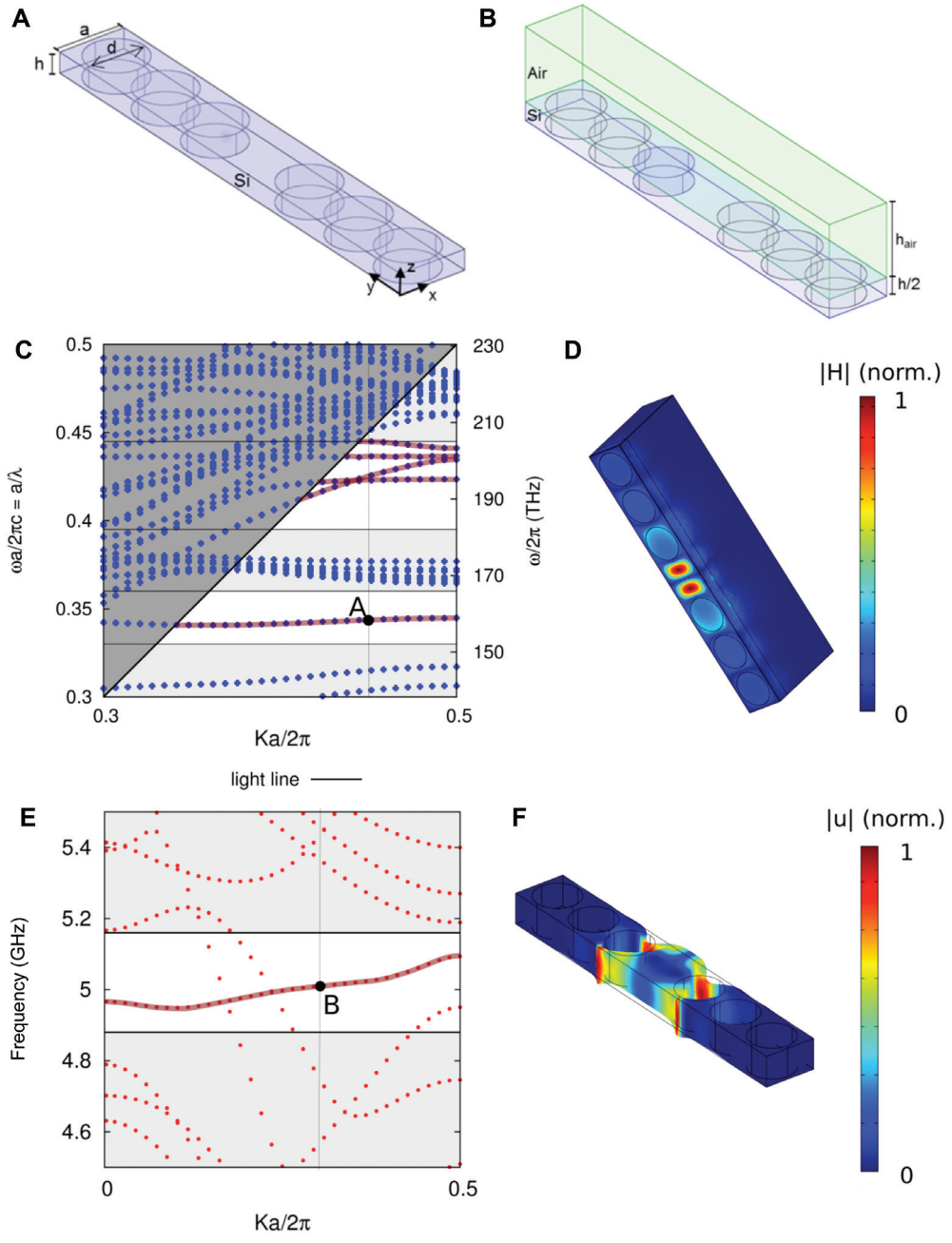

Figure 8 A 2D square lattice phoxonic crystal waveguide, as adapted from [14]. The geometrical parameters are pitch a=651 nm, thickness h=390 nm, and hole diameter d=560 nm. The waveguide width is chosen as w=0.9a. Phononic and photonic propagation characteristics are obtained with the finite element method, using super-cells and two-dimensional periodic boundary conditions on the lateral sides. (A) For elastic waves, only the solid part (silicon) needs to be meshed. Traction-free boundary conditions are applied at the top and the bottom surfaces. (B) For photonic modes, the vacuum or air inside the holes and surrounding the slab needs to be taken into account. (C) The photonic band structure allows one to identify the guided optical waves in the solid core. The light cone is shown as the dark gray region. Two photonic band gaps for guided waves appear in white. The bands supporting waves guided thanks the photonic band gap effect are shown with solid lines. (D) Modal distribution for the optical eigenmode at 165 THz. The modulus of the magnetic field vector H is presented for the reduced wavenumber value $ka/2\pi$=0.45. (E) A complete phononic band gap exists for frequencies around 5 GHz, as shown in white in the phononic band structure. A slow acoustic wave guided in the solid core within the phononic band gap is depicted with a solid line. (F) The modal distribution of this guided wave is shown for $Ka/2\pi$=0.3. The color bar is for the modulus of the total displacement while the deformation of the mesh is proportional to the algebraic displacements.

band gap, but also to obtain simultaneous slow light (at telecom wavelengths) and slow sound propagation, so as to maximize energy transfer during photon-phonon interactions. Figure 8C shows the photonic band structure (even parity modes) of the waveguide. Especially interesting is the low band gap appearing around the reduced frequency 0.35. In this frequency range, only one guided branch appears, and it shows flat dispersion (low group velocity). The modal distribution of the corresponding Bloch wave is shown in Figure 8D, for the particular value of the reduced wave number $ka/2\pi$=0.35. Figure 8E shows the phononic band structure of the defect-based phoxonic crystal waveguide around 5 GHz. A total of up to four additional branches appear in the band gap region (indicated in white). Each of them supports a mode that is confined within the solid core by the phononic band gap effect. The most interesting mode is the one with the flattest dispersion (lowest group velocity), appearing around 5 GHz for all axial wave vectors. The modal distribution of a particular guided mode is shown in Figure 8F, for $ka/2\pi$=0.3. Confinement inside the core by the phononic band gap effect is seen to be very effective.

The overlap-integral approach straightforwardly allows one to estimate the PE and MI contributions to the AO coupling, as described in detail for phoxonic crystal cavities in Section 4.1. Since the generation of phonons from the incident optical waves is of great interest here, we instead briefly outline the ES process as described in Refs. [70, 78]. Assuming two counter propagative optical waves with the same modal distribution but small frequency detuning Ω are launched inside the phoxonic crystal waveguide, see Eq. (13) with $\omega_2=\omega_1+\Omega$ and $k_2\approx -k_1$, the elastodynamic equation (16) can be solved for the displacement of the elastic wave by fixing the acoustic wave vector $K=2k_1$ and scanning the frequency detuning Ω. The right-hand side of the elastodynamic equation is the divergence of the electrostrictive force of purely optical origin, as given by Eq. (17). The spatial phonon distribution is thus obtained directly as a result of the applied optical force, and never has to be assumed to arise from a particular normal elastic mode of the waveguide. In practice, the guided optical waves are first obtained, e.g., using a 3D FEM model. In order to simulate a realistic AO interaction, elastic losses are incorporated in the ES model by considering a complex elastic tensor $c_{ijkl}+i\rho_{ijkl}$ where ρ_{ijkl} is a viscosity tensor [79]. This loss model is compatible with the usual assumption that the *Qf* product (with $f=\Omega/2\pi$) is constant for a given material. For silicon wafers, a value $Qf=5\cdot10^{13}$ Hz is considered at room temperature, as estimated from experiments. At a phonon frequency of 5 GHz, the intrinsic Q-factor is thus around 10,000. In this case, loss is considered to arise only from coupling with thermal phonons, and thus depends directly on the temperature. Imperfections of the phoxonic crystal fabrication, such as roughness of interfaces, are thus not taken into account. The computed ES gain spectrum as a function of frequency, i.e., the theoretical Brillouin spectrum, is shown in Figure 9A. This ES gain is obtained as the total elastic energy per unit length in the phonon distribution, by integration of the elastic energy density over the waveguide section. Since the reduced photon wavenumber is $ka/2\pi$=0.35, the reduced phonon wavenumber is $Ka/2\pi$=0.7 from the phase-matching condition. Folding at the boundary of the first Brillouin zone implies that we can simply consider $Ka/2\pi$=0.3. The elastic energy density of the confined phonon excited at resonance is depicted in Figure 9C. There is a clear correspondence with the phonon mode shown in Figure 8F, which was obtained independently from the phononic band structure. The other phonons in the band structure, however, do not give rise to any appreciable Brillouin gain. This is a direct illustration of the fact that band structure calculations alone are not sufficient and that invaluable information can be obtained from the detailed spectral distribution of the Brillouin gain.

5 Foreseen applications

5.1 Applications of light-sound interaction in nanoscale cavities

A key phenomenon arising from the light-sound coupling in a small volume is the possibility to cool a phoxonic cavity down to its quantum mechanical ground state. The interesting point is that cooling the cavity so that it is virtually empty of phonons would enable to observation of quantum phenomena that otherwise would be obscured by thermal noise. To explain the fundamentals of laser cooling, let us consider a phoxonic cavity that supports an optical resonance (frequency ω_0 and decay rate κ) and a mechanical resonance (frequency Ω_0 and damping Γ_m). We assume that the cavity is excited with a laser source whose frequency ω_L is slightly red-shifted from the cavity resonance. If the laser is tuned at a frequency a distance equal to the mechanical mode, $\omega_L=\omega_0-\Omega_0$, resonant phonons will provide the additional amount of energy so that photons can enter in resonance at ω_0 via a dynamic back-action process originated in the radiation pressure force exerted by the photons on the cavity walls [1, 3, 4, 80]. Note that other types of AO interaction such as ES [81], which was discussed in Section 3, or even photothermal pressure

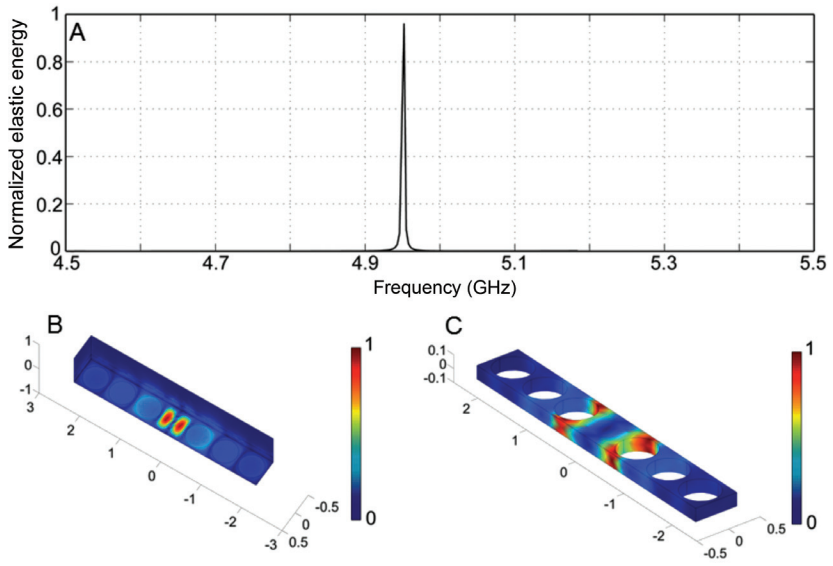

Figure 9 Photon-phonon interaction in a 2D phoxonic crystal slab waveguide.
(A) ES gain as a function of detuning frequency for the square-lattice phoxonic crystal waveguide of Figure 8.The excitation of a single resonant phonon at 4.95 GHz is predicted. (B) Magnetic field distribution of the fundamental optical mode launched in the phoxonic crystal waveguide, with $ka/2\pi$=0.35. (C) Absolute displacement distribution of the resonant phonon, with $Ka/2\pi$=0.3 (i.e., for K=2k and after band folding at the edge of the first Brillouin zone).

(not discussed in this work) [82], may also be the mechanism activating the back-action process. In a light-sound interaction framework, we can consider that an incoming photon interacts with a phonon created by some AO force to produce a higher-frequency (anti-Stokes) photon resonant with the cavity (see Figure 10A). Using this approach, usually known as sideband cooling, laser-induced cooling via radiation pressure of mechanical resonators embedded into high-Q factor optical cavities was demonstrated some years ago [80, 83, 84]. Subsequent approaches made use of cavities that were able to confine simultaneously the involved photons and phonons [85, 86]. In order to reach the mechanical ground state, working in the resolved sideband (or "good-cavity") regime, in which the optical bandwidth of the cavity should be smaller than the resonance frequency of the phonon mode ($\kappa<\Omega_0$), becomes a key issue (see Figure 10B) [85]. It deserves to be mentioned that cooling down to the ground state is also possible in the "bad cavity" limit by means of cold-damping quantum-feedback cooling [87]. Resolved-sideband cooling was first demonstrated in a microtoroidal cavity [85] and further developments enabled reaching the ground state by demonstrating a phonon occupancy number lower than unity in a microwave resonator [86] and also in a silicon 1D phoxonic crystal cavity [7]. Phoxonic crystal cavities are a very interesting platform to implement sideband cooling, as demonstrated in [7], since they allow for high optical Q-factors (>10^4) and mechanical resonances in the GHz regime, which means that the resolved sideband regime can be easily reached. Interestingly, using the same approach but with the input laser blue-detuned with respect of the cavity resonance (see Figure 10C), amplification of phonons inside the cavity becomes feasible, which results in the amplification of the mechanical oscillations (heating) and ultimately to self-oscillation of the resonator when the total mechanical damping rate vanishes [6, 83]. More details about sideband cooling of mechanical cavities can be found in a recent review [3].

The optical wavelength shift as a consequence of the interaction of the incoming light with cavity phonons can also be used for coherent optical wavelength conversion [88], a key functionality in future all-optical communication networks. In this process, a phoxonic cavity supporting two high-Q factor photonic modes is necessary. The wavelength shift resulting from the conversion process is of the order of the spacing between the photonic resonances, which in principle can be tailored at will. In fact, AO interactions in phoxonic nanostructures constitute a very interesting mechanism for all-optical processing of information, not only in cavities, but also in waveguides as shown in Section 5.2.

Photonic and phononic cavities can also be separately used as ultrasensitive sensors that can ultimately achieve detection of even single molecules. In both cases, typically a change of the resonance frequency under the presence of a target substance is detected, so a key requirement is

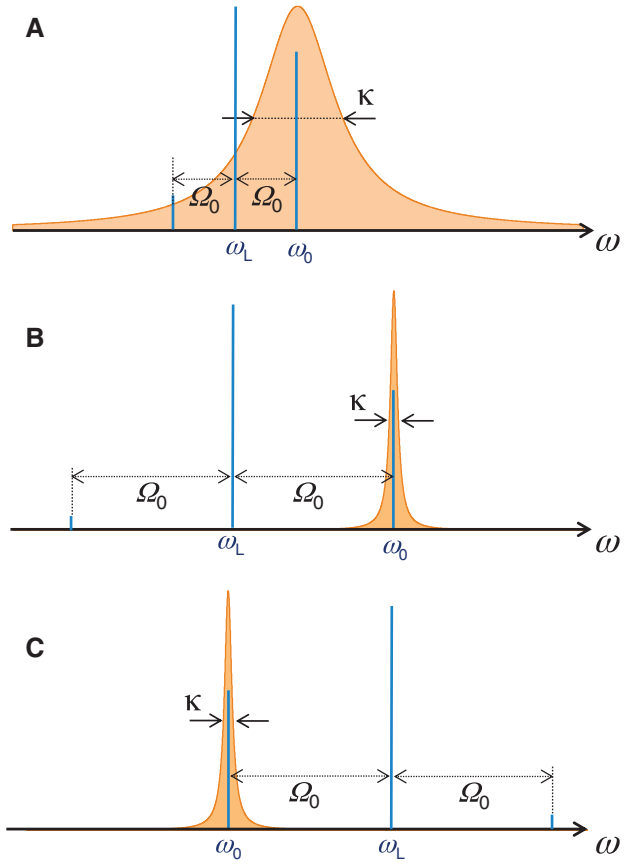

Figure 10 Frequency spectrum picture of the sideband cavity cooling phenomenon in phoxonic cavities.
(A) A cavity supporting an optical resonance (ω_0) and a mechanical resonance (Ω_0) is fed by a laser (ω_L) red-shifted from the optical resonance a frequency equal to Ω_0. In the "bad cavity" limit, the mechanical resonance is smaller than the optical decay rate, $\Omega_0<\kappa$. Incident photons are inelastically scattered by cavity phonons at frequencies ω_L-Ω_0 (lower sideband) and $\omega_L+\Omega_0=\omega_0$ (upper sideband). The asymmetric sideband spectrum is a result of the asymmetry of the feeding signal with respect to the photonic density of states of the cavity (colored region). The increase of frequency of an incoming photon removes a cavity phonon, which results in the cooling of the cavity. (B) In the "good cavity" limit, the mechanical resonance is larger than the optical decay rate, $\Omega_0>\kappa$, which means that the cavity enters the resolved-sideband regime which allows for cooling down the fundamental ground state of the cavity. (C) In the case of blue detuning, the process is similar but phonons are created instead of removed, leading to amplification of the mechanical mode.

a very high-Q factor (the minimum frequency shift that can be detected is of the order of the full-wave half-maximum of the resonance). However, the measured physical property is different in each case. In photonics, it is the refractive index of the targeted substance what shifts the sensor response. A typical figure of merit is the resonance wavelength shift per refractive index unit (measured in nm/RIU). A very small modal volume is also an important requirement, so that tiny amounts of matter (eventually a single molecule) can strongly modify the photonic response, which will be affected by small changes in the refractive index of the cavity surroundings. Using this approach, nanoscale sensors based on 2D photonic crystal cavities in gas [89] and liquid environments [90] with sensitivities beyond 1000 nm/RIU have been demonstrated.

In acoustics/mechanics, the physical properties that can be tested are the density and the elastic modulus of the applied substance. This way, micro- and nanomechanical resonators can be employed as mass sensors. Such devices can work both in gas and liquid environments in which typically the small nanoparticles to be detected are immersed so that some of them can be attached to the resonator. Nanomechanical mass sensors need to have a very small mass since, when working in the dynamic mode, the shift in the resonance is proportional to the ratio between the mass of the amount of matter to be tested and the mass of the resonator. Achieving ultralight resonators would also result in a very high resonance frequency (some GHz). For instance, it has been recently shown that a nanomechanical resonator consisting of a 150-nm-long carbon nanotube vibrating at a frequency of 1.8 GHz can detect single-molecule adsorption events when placed in high vacuum [91]. Such high resonance frequencies would pave the way towards sensitive mass sensors working under ambient conditions, since air damping degradation of the mechanical Q factor diminishes as the frequency increases [92]. Therefore, the acoustic modes at GHz frequencies that can exist in phoxonic crystal cavities could also perform in a similar way and be used as ultrasensitive mass sensors [6]. Moreover, such a mass sensor could be all-optically actuated (for instance, by using a blue-detuned laser so that the mechanical motion gets amplified, see Figure 10C) because vibration can be induced and detected optically, so the sensor speed would outperform those relying on electrical readout schemes. High-amplitude operation of such devices is another key requirement in order to operate at room-temperature [93]. However, phoxonic crystal cavities suffer from small dynamic range even though its motion gets amplified as a result of their ultrasmall dimension. Although recent approaches have shown routes to drive nanomechanical structures at large amplitude via optical fields [93], this still remains a challenge in phoxonic crystal cavities. Nevertheless, it can be envisaged that properly-actuated phoxonic crystal cavities would combine the best of the two worlds, giving rise to the implementation of dual photonic-phononic sensors able to detect ultrasmall changes in the refractive index (photonic sensing) and mass (phononic sensor) of its surroundings.

Besides their use as mass sensors, acoustic/mechanical resonators can also be used to detect tiny changes in the density of the gas/liquid environment surrounding them. In such a case, they would perform in the same way as their photonic counterparts: a small change of the impedance of the surroundings is detected. Using such an approach, a highly sensitive acoustic sensor in a liquid environment in phononic crystal structures working in the MHz regime has been reported [94]. Adding up the photonic functionality, we could easily get a phoxonic crystal structure for dual liquid sensing in the photonic and phononic domains simultaneously. Here, we use numerical simulations to illustrate the potential of phoxonic crystal cavities for dual liquid sensing applications. To make a dual phoxonic sensor, one needs to design a structure in which the transmission coefficient displays well-defined spectral features that are very sensitive to the acoustic/optic velocity of the infiltrating liquid. These features should be relatively isolated in frequency in order to allow the sensing of the probed parameter on a sufficiently broad range. We consider an infinite 2D phoxonic crystal made of periodic holes on silicon in which one row of holes presents a bigger radius (r/a=0.4) compared to the regular ones (r/a=0.25). For light/sound incidence normal to the defect, it can be considering as acting as a phoxonic cavity. In Figure 11A, we show the acoustic transmission through the 2D phononic crystal when the infinite row of cavities is filled with water. Due to the water filled cavity, a succession of peaks and dips appear in the transmission spectrum labeled with A, B, C.... The shaded blue area corresponds to the phononic band gap. In Figure 11B, we plot the evolution of the dip (A) when changing the acoustic velocity c_l of the liquid with respect to water as reported in the table of Figure 11. The frequencies of the resonant modes increase by increasing the sound velocity of the liquid and the relative shift in frequency has almost the same order of magnitude as the relative shift in the velocity c_l.

As mentioned before, the main interest of this dual sensor is related to the possibility of sensing the refractive index (or the velocity of light) simultaneously with the sound velocity in the liquid. Indeed, the change in the size of the holes allows the appearance of a localized mode inside the band gap of the photonic crystal whose frequency is sensitive to the index of refraction of the liquid. Figure 11C shows the photonic transmission for TE-polarized light, where one can see the existence of a localized mode inside the photonic band gap. When the holes in the cavity region are filled with different liquids, the transmission peak shifts proportionally to the liquid refractive index (see Figure 11D), which demonstrates the use of the structure as a photonic sensor. Let us notice that to work at the telecom wavelength of 1550 nm, the period of the photonic crystal should be in the range of

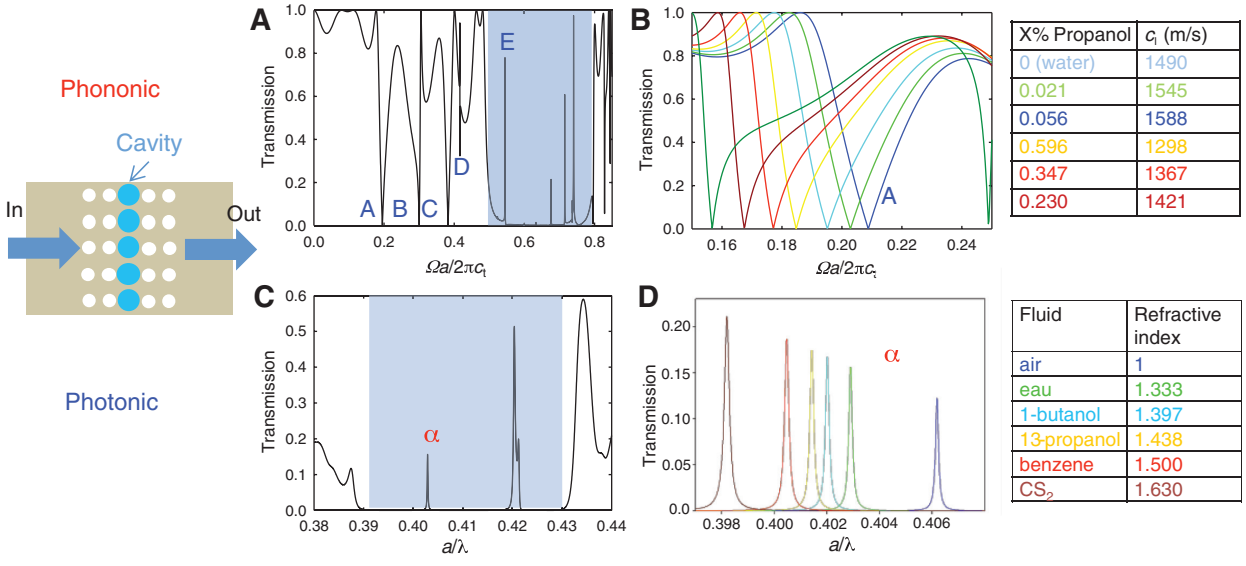

Figure 11 Schematic representation of a dual phoxonic crystal sensor consisting of a 2D square lattice of periodic holes with radius r/a=0.25 on a silicon substrate where one row of holes with radius r/a=0.4 is infiltrated with a liquid.
(A) Phononic transmission curve (c_t=5844 m/s is the sound speed in silicon in the crystallographic direction [100]). (B) Evolution of the dips A as a function of the sound velocity of the liquid reported in the handed table. (C) Photonic transmission curve in normalized frequency units. (D) Evolution of the transmitted peaks (mode α) as a function of the refractive index of the liquid reported in the table.

650 nm and, consequently, the gap of the corresponding phononic crystal falls around 5.5 GHz, in close agreement with other phoxonic structures shown above. With these parameters, we have obtained a phononic sensitivity $S=\frac{\Delta f}{\Delta c_l}=2.0\ \mathrm{MHz}/(ms^{-1})$, and a photonic one of $S=\frac{\Delta\lambda}{\Delta n}=60\ nm/RIU$, comparable to those reported in the literature. It has to be mentioned that this kind of dual phoxonic sensor does not actually rely on the AO interaction inside the defect but provides a simultaneous response for both photons and phonons, meaning that we can get information about the electromagnetic and acoustic properties of a given substance in a single measurement. However, it can be thought that if a given substance changes both the photonic and phononic response of the device, it will also affect the interaction of both kinds of waves when introduced in the cavity, so we would get additional information on the substance to be analyzed. In other words, the sensor would provide quantitative information about how the substance modifies the electromagnetic and acoustic properties of the system as well as the resulting photon-phonon interaction inside the cavity.

5.2 Applications of light-sound interaction in nanoscale waveguides

Efficient coupling between phonons and photons inside integrated waveguides via Brillouin effects would open up a host of wide-band all-optical signal processing capabilities with CMOS compatible silicon photonics, including pulse storage [95], opto-acoustic sensing [96], coherent frequency comb generation [97], coherent beam combining [98], on-chip Brillouin laser implementation [72, 99], and ultra-compact slow-light device fabrication [75, 97]. The very strong spatial confinement that can be obtained within a nanoscale waveguide may further be combined with low group velocities for both sound and light waves arising in phoxonic crystal structures in order to further enhance AO effects, as we have seen in Section 4.2. The phoxonic crystal waveguide in Figure 8 supports slow light propagation with group index $n_g \approx 25$ (i.e., 25 times slower than in a vacuum) [14]. Around the 5 GHz resonant phonon frequency shown in Figure 8, the phonon group velocity varies around a mean value of 180 m/s, more than 30 times smaller than the speed of any bulk wave in silicon and actually less than the speed of sound in air. Since this optimization was the first of its type, it is likely that even better configurations for phoxonic crystal waveguides supporting joint slow light and sound propagation can be found in the future [22]. The simultaneous control of phononic and photonic group velocity in a silicon chip thus has the potential to vastly enhance opto-acoustic and acousto-optic interactions within silicon integrated chips, though an experimental demonstration still remains to be made. A detailed theoretical study of the group velocity scaling of AO interactions inside phoxonic crystal waveguides has not yet been reported, to the best of our knowledge. We can, however, make a conjecture based on facts known from related areas. First, the material figure of merit of guided-wave acousto-optics, $M2=n^3p^6/\rho v^2 v_g$, where n is the optical index, v is the acoustic phase velocity, v_g is the acoustic group velocity, and ρ is the mass density, is known to scale with the inverse of the acoustic group velocity. Second, coupled-wave equations for the amplitudes of the optical waves in equations (14, 15) are known to scale with the inverse of the optical group velocity. As a result, we conjecture that the strength of AO interactions in phoxonic crystal waveguides should scale with the inverse of both photon and phonon group velocities.

Optical delay systems or more generally optical memories are considered as the main obstacle to the development of all-optical information processing. Light pulses can be stored in the form of acoustic phonons driven by the Brillouin scattering process with a damping time of about 10 ns in silica optical fibers. In Figure 12, we depict the Brillouin storage process within a phoxonic crystal waveguide, as adapted from the optical fiber scheme introduced in Ref. [25]. In Figure 12A, an intense write light wave is used to store a data sequence as an acoustic wave through the Brillouin scattering process during the phonon lifetime (Figure 12B). In the case of silica fibers, it is thus possible to store a pulse with duration of 100 ps for about 10 ns. This delay does not only depend on the lifetime of the acoustic wave. However, it is possible to regenerate the acoustic wave by sending regularly optical energy through the Brillouin scattering process [91]. As we represent in Figure 12D, an intense read light pulse is injected to read the stored information [25]. Unfortunately, this technique requires a very efficient AO interaction over very short propagation lengths, which is difficult to achieve with silica. The implementation of this method in standard optical fibers therefore requires very high optical powers that are hardly compatible with industrial implementations [100]. The stronger Brillouin gain that can be expected with silicon [15] combined with joint slow light and sound propagation in phoxonic crystal waveguides could be favorable for the realization of integrated optical delay lines with small footprints and reasonable power levels.

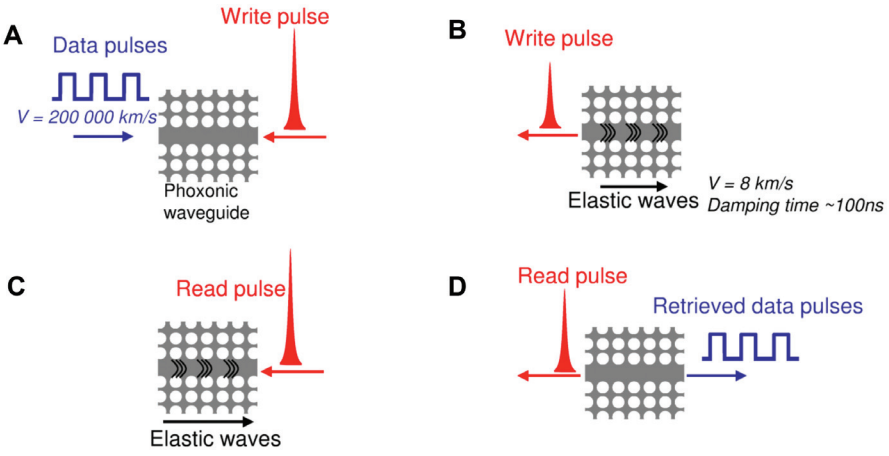

Figure 12 Schematic of a delay line for light pulses designed to store information in the form of acoustic phonons within a silicon phoxonic crystal waveguide, as adapted from the optical fiber scheme introduced in [25].
(A) An intense write light wave whose frequency is shifted by the acoustic resonance of the material relative to the data pulse frequency is used to store a data sequence as an acoustic wave through the Brillouin scattering process. (B) The information stored by the acoustic wave has a lifetime of approximately 100 ns in silicon, as limited by phonon decay. (C) In order to read the stored information, an intense read light pulse with the same frequency as the write pulse is injected at a later time. (D) The interaction of the reading pulse with the acoustic phonon creates a light pulse train reproducing the original data.

6 Conclusions and prospects

In this paper we have described a full set of analytical tools that allow for modeling the AO interaction between light (photons) and sound (acoustic phonons) in nanoscale structures. Different kinds of interactions between photons and phonons are explained and properly considered to obtain appropriate analytical expressions to model them. Specifically, we differentiate between being volume (PE, ES) and surface (MI, radiation pressure) AO effects as well as between effects being launched by an acoustic (PE, MI) or an optical (ES, radiation pressure) wave. Together with the wide variety of numerical methods commonly employed to obtain the fields and the dispersion relations in both photonic and phononic nanostructures, these tools set the basis to design novel phoxonic structures for enhanced AO interaction in nanoscale cavities and waveguides. Moreover, the methods described here are general and can be applied to any kind of host material or structure, so its use is not restricted to silicon phoxonic/OM crystals. We have also provided a set of phoxonic structures providing photonic as well as phononic bandgaps that can be used to implement cavities and waveguides which enable strong photon-phonon interaction. Finally, we have described some applications in which phoxonic crystal structures can play a key role and, as so, the methods explained in this paper can be of interest, such as sideband cavity cooling, all-optical processing or dual phoxonic sensors. In general, enhancing the AO interaction at the nanoscale will lead to a new generation of miniaturized AO devices like integrated optical storage and delay line elements based on enhanced SBS. Moreover it could boost the importance of the new field of optomechanics enabling hybrid photonic-phononic circuits controlled through OM elements.

In order to continue the evolution of the field and take maximum profit of the light-sound interaction in nanoscale structures, some next steps can be easily been foreseen. For instance, phoxonic structures displaying full phononic bandgaps have been only recently demonstrated [32, 33]. However, the full potential of such structures, which should extremely reduce acoustic radiation losses in real devices, is still to be unveiled. For the particular case of AO cavities, most experiments showing light-sound interaction in phoxonic cavities have employed a tapered fiber put in close proximity of the cavity to excite the confined light modes. This approach exhibits some important limitations, mainly the inability to drive multiple cavities at the same time, therefore constraining a key feature of OM crystals. Therefore, it would be highly desirable to access them via integrated optical waveguides. However, there have been only a few experiments reporting AO coupling in phoxonic cavities using this approach [26]. Regarding waveguides, the demonstration of AO interaction in phoxonic waveguides as well as its predicted enhancement via slow photons and phonons has not been demonstrated so far. Finally, it would be highly interesting to combine the worlds of phoxonic/OM crystals and plasmonics. Metallic

nanostructures provide strong confinement of the electric [101] and even magnetic field [102] in deep subwavelength regions via excitation of localized surface plasmon resonances. Interestingly, they also exhibit vibrational resonances in the GHz regime [103]. Therefore, the insertion of plasmonic nanostructures into phoxonic structures such as cavities would extremely enhance the AO interaction via the high-field confinement inherent to plasmonics whilst the optical and acoustic responses of the metallic nanostructure would be fully modified by the existence of a phoxonic bandgap. Additionally, this approach would enable the observation of AO interaction in subwavelength regions beyond the diffraction limit. We foresee new and exciting physical phenonema arising from such a combination.

Acknowledgments: We acknowledge funding from the European Community's Seventh Framework Programme (FP7/2007–2013) under grant agreement number 233883 (TAILPHOX).

References

[1] Korpel A. Acousto-optics. 2nd ed. New York: CRC Press, 1996.
[2] Kippenberg TJ, Vahala KJ. Cavity optomechanics: back-action at the mesoscale. Science 2008;321:1172–6.
[3] Aspelmeyer M, KippenbergTJ, Marquardt F. Cavity Optomechanics, arXiv:1303.0733.
[4] Favero I, Karrai K. Optomechanics of deformable optical cavities. Nat Photon 2009;3:201–5.
[5] Eichenfield M, Camacho R, Chan J, Vahala KJ, Painter O. A picogram- and nanometre-scale photonic-crystal optomechanical cavity. Nature 2009;459:550–5.
[6] Eichenfield M, Chan J, Camacho RM, Vahala KJ, Painter O. Optomechanical crystals. Nature 2009;462:78–82.
[7] Chan J, Mayer Alegre TP, Safavi-Naeini AH, Hill JT, Krause A, Gröblacher S, Aspelmeyer M, Painter O. Laser cooling of a nanomechanical oscillator into its quantum ground state. Nature 2011;478:89–92.
[8] Safavi-Naeini AH, Mayer Alegre TP, Chan J, Eichenfield M, Winger M, Lin Q, Hill JT, Chang DE, Painter O. Electromagnetically induced transparency and slow light with optomechanics. Nature 2011;472:69–73.
[9] Weis S, Rivière R, Deléglise S, Gavartin E, Arcizet O, Schliesser A, Kippenberg TJ. Optomechanically induced transparency. Science 2010;300:1520–3.
[10] Gavartin E, Braive R, Sagnes I, Arcizet O, Beveratos A, Kippenberg TJ, Robert-Philip I. Optomechanical coupling in a two-dimensional photonic crystal defect cavity. Phys Rev Lett 2011;106:203902.
[11] Rolland Q, Oudich M, El-Jallal S, Dupont S, Pennec Y, Gazalet J, Kastelik JC, Leveque G, Djafari-Rouhani B. Acousto-optic couplings in two-dimensional phoxonic crystal cavities. Appl Phys Lett 2012;101:061109.
[12] Pennec Y, Djafari-Rouhani B, El-Boudouti EH, Li C, El-Hassouani Y, Vasseur J, Papanikolaou N, Benchabane S, Laude V, Martinez A. Simultaneous existence of phononic and photonic band gaps in periodic crystal slabs. Opt Express 2010;18:14301–10.
[13] Mohammadi S, Eftekhar AA, Khelif A, Adibi A. Simultaneous two-dimensional phononic and photonic band gaps in optomechanical crystal slabs. Opt Express 2010;18:9164–72.
[14] Laude V. Beugnot JC, Benchabane S, Pennec Y, Djafari-Rouhani B, Papanikolaou N, Escalante JM, Martinez A. Simultaneous guidance of slow photons and slow acoustic phonons in silicon phoxonic crystal slabs. Opt Express 2011;19:9690–8.
[15] Rakich PT, Reinke C, Camacho R, Davids P, Wang Z. Giant Enhancement of stimulated brillouin scattering in the subwavelength limit. Phys Rev X 2012;2:011008.
[16] Tomes M, Carmon T. Photonic micro-electromechanical systems vibrating at X-band (11-GHz) rates. Phys Rev Lett 2009;102:113201.
[17] DholakiaK, Čižmár T. Shaping the future of manipulation. Nat Photon 2011;5:335.
[18] Joannopoulos JD, Villeneuve PR, Fan S. Photonic crystals: putting a new twist on light. Nature 1997;386:143–9.
[19] Pennec Y, Vasseur J, Djafari-Rouhani B, Dobrzynski L, Deymier PA. Two-dimensional phononic crystals: examples and applications. Surf Sci Rep 2010;65:229–91.
[20] Maldovan M. Sound and heat revolutions in phononics. Nature 2013;503:209–17.
[21] Maldovan M, Thomas E. Simultaneous localization of photons and phonons in two-dimensional periodic structures. Appl Phys Lett 2006;88:251907.
[22] Escalante JM, Martínez A, Laude V. Design of single-mode waveguides for enhanced light-sound interaction in honeycomb-lattice silicon slab. J Appl Phys 2014;115:064302.
[23] Nunnenkamp A, Børkje K, Girvin SM. Single photon optomechanics. Phys Rev Lett 2011;107;063602.
[24] Li Y, Zheng J, Gao J, Shu J, Aras MS, Wong CW. Design of dispersive optomechanical coupling and cooling in ultra-high-Q/V slot-type photonic crystal cavities. Opt Express 2010;18:23844–56.
[25] Zhu Z, Gauthier DJ, Boyd RW. Stored light in an optical fiber via stimulated Brillouin scattering. Science 2007;318:1748–50.
[26] Bochmann J, Vainsencher A, Awschalom DD, Cleland AN. Nanomechanical coupling between microwave and optical photons. Nat Phys 2013;9:712–6.
[27] Sadat-Saleh S, Benchabane S,Baida FI, Bernal MP, Laude V. Tailoring simultaneous photonic and phononic band gaps. J Appl Phys 2009;106:074912.
[28] Fan L, Sun X, Xiong C, Schuck C, Tang HX. Aluminum nitride piezo-acousto-photonic crystal nanocavity with high quality factors. Appl Phys Lett 2013;102:153507.
[29] Benchabane S, Gaiffe O, Ulliac G, Salut R, Achaoui Y, Laude V. Observation of surface-guided waves in holey hypersonic phononic crystal. Appl Phys Lett 2011;98:171908.
[30] Fuhrmann DA, Thon SM, Kim H, Bouwmeester D, Petroff PM, Wixforth A, Krenner HJ. Dynamic modulation of photonic crystal nanocavities using gigahertz acoustic phonons. Nat Photon 2011;5:605–9.
[31] Psarobas IE, Papanikolaou N, Stefanou N, Djafari-Rouhani B, Bonello B, Laude V. Enhanced acousto-optic interactions in a one-dimensional phoxonic cavity. Phys Rev B 2010;82:174303.

[32] Gomis-Bresco J, Navarro-Urrios D, Oudich M, El-Jallal S, Griol A, Puerto D, Chavez E, Pennec Y, Djafari-Rouhani B, Alzina F, Martínez A, Sotomayor Torres CM. A 1D Optomechanical crystal with a complete phononic band gap. Nat Commun 2014;5:4452.
[33] Safavi-Naeini AH, Hill JT, Meenehan S, Chan J, Groeblacher S, Painter O. Two-dimensional phononic-photonic bandgap optomechanical crystal cavity. Phys Rev Lett 2014;112:153603.
[34] Sainidou R, Stefanou N, Modinos A. Formation of absolute frequency gaps in three-dimensional solid phononic crystals. Phys Rev B 2002;66:212301.
[35] Trigo M, Bruchhausen A, Fainstein A, Jusserand B, Thierry-Mieg V. Confinement of acoustical vibrations in a semiconductor planar phonon cavity. Phys Rev Lett 2002;89:227402.
[36] Russell P. Photonic crystal fibers. Science 2003;299:358–62.
[37] Russell PStJ, Marin E, Diez A, Guenneau S, Movchan AB. Sonic band gaps in PCF preforms: enhancing the interaction of sound and light. Opt Express 2003;20:2555–60.
[38] Laude V, Khelif A, Benchabane S, Wilm M, Sylvestre T, Kibler B, Mussot A, Dudley JM, Maillotte H. Phononic band-gap guidance of acoustic modes in photonic crystal fibers. Phys Rev B 2005;71:045107.
[39] Foresi JS, Villeneuve PR, Ferrera J, Thoen ER, Steinmeyer G, Fan S, Joannopoulos JD, Kimerling LC, Smith HI, Ippen EP. Photonic-bandgap microcavities in optical waveguides. Nature 1997:390:143–5.
[40] Johnson SG, Fan S, Villeneuve PR, Joannopoulos JD, Kolodziejski LA. Guided modes in photonic crystal slabs. Phys Rev B 1999;60:5751.
[41] Akahane Y, Asano T, Song BS, Noda S. High-Q photonic nanocavity in a two-dimensional photonic crystal. Nature 2003;425:944–7.
[42] Notomi M, Yamada K, Shinya A, Takahashi J, Takahashi C, Yokohama I. Extremely large group-velocity dispersion of line-defect waveguides in photonic crystal slabs. Phys Rev Lett 2001;87:253902.
[43] Hsu FC, Lee CI, Hsu JC, Huang TC, Wang CH, Chang P. Acoustic band gaps in phononic crystal strip waveguides. Appl Phys Lett 2010;96:051902.
[44] Chan J, Safavi-Naeini AH, Hill JT, Meenehan S, Painter O. Optimized optomechanical crystal cavity with acoustic radiation shield. Appl Phys Lett 2012;101:081115.
[45] Pennec Y, Djafari-Rouhani B, Li C, Escalante JM, Martinez A, Benchabane S, Laude V, Papanikolaou N. Band gaps and cavity modes in dual phononic and photonic strip waveguides. AIP Advances 2011;1:041901.
[46] Safavi-Naeini AH, Painter O. Design of optomechanical cavities and waveguides on a simultaneous bandgap phononic-photonic crystal slab. Opt Express 2010;18:14926–43.
[47] El Hassouani Y, Li C, Pennec Y, El Boudouti EH, Larabi H, Akjouj A, Bou Matar O, Laude V, Papanikolaou N, Martinez A, Djafari-Rouhani B. Dual phononic and photonic band gaps in a periodic array of pillars deposited on a thin plate. Phys Rev B 2010;82:155405.
[48] Papanikolaou N, Psarobas IE, Stefanou N. Absolute spectral gaps for infrared light and hypersound in three-dimensional metallodielectric phoxonic crystals. Appl Phys Lett 2010;96:231917.
[49] Ma TX, Wang YS, Wang YF, Su XX. Three-dimensional dielectric phoxonic crystals with network topology. Opt Express 2013;21:2727–32.
[50] Akimov AV, Tanaka Y, Pevtsov AB, Kaplan SF, Golubev VG, Tamura S, Yakovlev DR, Bayer M. Hypersonic Modulation of light in three-dimensional photonic and phononic band-gap materials. Phys Rev Lett 2008;101:033902.
[51] Royer D, Dieulesaint E. Elastic waves in solids. New York, Wiley, 1999.
[52] Xu J, Stroud R. Acousto-optic devices: principles, design, and applications. New York, Wiley, 1992.
[53] Laude V. General solution of the coupled-wave equations of acousto-optics. J Opt Soc Am A 2003;20:2307–14.
[54] Chiao RY, Townes C, Stoicheff BP. Stimulated Brillouin Scattering and Coherent Generation of Intense Hypersonic Waves. Phys Rev Lett 1964;12:592.
[55] Eichenfeld M, Chan J, Safavi-Naeini AH, Vahala KJ, Painter O. Modeling dispersive coupling and losses of localized optical and mechanical modes in optomechanical crystals. Opt Express 2009;17:20078–98.
[56] Johnson SG, Ibanescu M, Skorobogatiy MA, Weisberg O, Joannopoulos JD, Fink Y. Perturbation theory for Maxwell's equations with shifting material boundaries. Phys Rev E 2002;65:066611.
[57] Povinelli M, Johnson SG, Loncar M, Ibanescu M, Smythe E, Capasso F, Joannopoulos JD. High-Q enhancement of attractive and repulsive optical forces between coupled whispering-gallery-mode resonators. Opt Express 2005;13:8286–95.
[58] Povinelli M, Loncar M, Ibanescu M, Smythe E, Johnson SG, Capasso F, Joannopoulos JD. Evanescent-wave bonding between optical waveguides. Opt Lett 2005;3042–4.
[59] Gorodetsky ML, Schliesser A, Anetsberger A, Deleglise S, Kippenberg TJ. Determination of the vacuum optomechanical coupling rate using frequency noise calibration. Opt Express 2010;18:23236–46.
[60] Agrawal GP. Nonlinear fiber optics. San Diego, Academic Press, 2001.
[61] Boyd RW. Nonlinear optics, 3rd ed. San Diego, Academic Press, 2008.
[62] Nelson DF. Electric, optic, and acoustic interactions in dielectrics. New York: John Wiley & Sons, 1979.
[63] Dainese P, Russell P, Joly N, Knight J, Wiederhecker G, Fragnito H, Laude V, Khelif A. Stimulated Brillouin scattering from multi-GHz-guided acoustic phonons in nanostructured photonic crystal fibres. Nat Phys 2006;2:388–92.
[64] El-Jallal S, Oudich M, Pennec Y, Djafari-Rouhani B, Makhoute A, Rolland Q, Dupont S, Gazalet J. Optomechanic interactions in two-dimensional Si and GaAs phoXonic cavities. J Phys Cond Matter 2014;26:015005.
[65] El-Jallal S, Oudich M, Pennec Y, Djafari-Rouhani B, Laude V, Beugnot JC, Martínez A, Escalante JM, Makhoute A. Analysis of optomechanical coupling in two-dimensional square lattice phoxonic crystal slab cavities. Phys Rev B 2013;88;205410.
[66] Papanikolaou N, Psarobas IE, Stefanou N, Djafari-Rouhani B, Bonello B, Laude V. Light modulation in phoxonic nanocavities. Microelectron Eng 2011;90:155–8.
[67] Almpanis E, Papanikolaou N, Gantzounis G, Stefanou N. Tuning the spontaneous light emission in phoxonic cavities. J Opt Soc Am B 2012;29:2567–74.
[68] Gantzounis G, Papanikolaou N, Stefanou N. Nonlinear interactions between high-Q optical and acoustic modes in dielectric particles. Phys Rev B 2011;83:214301.

[69] Rakich PT, Davids P, Wang Z. Tailoring optical forces in waveguides through radiation pressure and electrostrictive forces. Opt Express 2010;18:14439–53.
[70] Laude V, Beugnot JC. Generation of phonons from electrostriction in small-core optical waveguides. AIP Advances 2013;3:042109.
[71] Shin H, Qiu W, Jarecki R, Cox JA, Olsson RH, Starbuck A, Wang Z, Rakich PT. Tailorable stimulated Brillouin scattering in nanoscale silicon waveguides. Nat Commun 2013;4:1944.
[72] Pant R, Poulton CG, Choi DY, McFarlane H, Hile S, Li E, Thévenaz L, Luther-Davies B, Madden SJ, Eggleton BJ. On-chip stimulated Brillouin scattering. Opt Express 2011;19:8285–90.
[73] Eggleton BJ, Poulton CG, Pant R. Inducing and harnessing stimulated Brillouin scattering in photonic integrated circuits. Adv Opt Photon 2013;5:536–87.
[74] Poulton CG, Pant R, Eggleton BJ. Acoustic confinement and stimulated Brillouin scattering in integrated optical waveguides. J Opt Soc Am B 2013;30:2657–64.
[75] Thévenaz L. Slow and fast light in optical fibres. Nat Photon 2008;2:474–81.
[76] Soljacic M, Joannopoulos JD. Enhancement of nonlinear effects using photonic crystals. Nat Mat 2004;3:211–9.
[77] Pennec Y, Djafari-Rouhani B, El Boudouti EH, Li C, El Hassouani Y, Vasseur JO, Papanikolaou N, Benchabane S, Laude V, Martinez A. Band gaps and waveguiding in phoxonic silicon crystal slabs. Chinese J Phys 2011;49:100–10.
[78] Beugnot JC, Laude V. Electrostriction and guidance of acoustic phonons in optical fibers. Phys Rev B 2012;86:224304.
[79] Moiseyenko RP, Laude V. Material loss influence on the complex band structure and group velocity in phononic crystals. Phys Rev B 2011;83:064301.
[80] Gigan S, Böhm HR, Paternostro M, Langer G, Hertzberg JB, Schwab KC, Bäuerle D, Aspelmeyer M, Seilinger A. Self-cooling of a micromirror by radiation pressure. Nature 2006;444:67.
[81] Bahl G, Tomes M, Marquardt F, Carmon T. Observation of spontaneous Brillouin cooling. Nat Phys 2012;8:203–207.
[82] Höghberger Metzger C, Karrai K. Cavity cooling of a microlever. Nature 2004;432:1002.
[83] Arcizet O, Cohadon PF, Briant T, Pinard M, Heidmann A. Radiation-pressure cooling and optomechanical instability of a micromirror. Nature 2006;444:71.
[84] Thompson JD, Zwickl BM, Jayich AM, Marquardt F, Girvin SM, Harrir JGE. Strong dispersive coupling of a high-finesse cavity to a micromechanical membrane. Nature 2008;452:72.
[85] Schliesser A, Riviere R, Anetsberger G, Arcizet O, Kippenberg TJ. Resolved sideband cooling of a micromechanical oscillator. Nat Phys 2008;4:415.
[86] Teufel JD, Donner T, Li D, Harlow JW, Allman MS, Cicak K, Sirois AJ, Whittaker JD, Lehnert KW, Simmonds RW. Sideband cooling of micromechanical motion to the quantum ground state. Nature 2011;475:359.
[87] Genes C, Vitali D, Tombesi P, Gigan S, Aspelmeyer M. Ground-state cooling of a micromechanical oscillator: comparing cold damping and cavity-assisted cooling schemes. Phys Rev A 2008;77:033804.
[88] Hill TF, Safavi-Naeini AH, Chan J, Painter O. Coherent optical wavelength conversion via cavity optomechanics. Nat Commun 2012;3:1196.
[89] Sünner T, Stichel T, Kwon SH, Schlereth TW, Höfling S, Kamp M, Forchel A. Photonic crystal cavity based gas sensor. Appl Phys Lett 2008;92:261112.
[90] Di Falco A, O'Faolain L, Krauss TF. Chemical sensing in slotted photonic crystal heterostructure cavities. Appl Phys Lett 2009;94:063503.
[91] Chaste J, Eichler A, Moser J, Ceballos G, Rurali R, Bachtold A. A nanomechanical mass sensor with yoctogram resolution. Nat Nanotechnol 2012;7:301–4.
[92] Li M, Tang HX, Roukes ML. Ultra-sensitive NEMS-based cantilevers for sensing, scanned probe and very high frequency applications. Nat Nanotechnol 2007;2:114–20.
[93] Bagheri M, Poot M, Li M, Pernice WPH, Tang HX. Dynamic manipulation of nanomechanical resonators in the high-amplitude regime and non-volatile mechanical memory operation. Nat. Nanotechnol 2011;6:726–32.
[94] Ke M, Zubtsov M, Lucklum R. Sub-wavelength phononic crystal liquid sensor. J Appl Phys 2011;110:026101.
[95] Schneider T, Junker M, Lauterbach KU. Theoretical and experimental investigation of Brillouin scattering for the generation of millimeter waves. J Opt Soc Amer B 2006;23:1012–9.
[96] Bahl G, Kim KH, Lee W, Liu J, Fan X, Carmon T. Brillouin cavity optomechanics with microfluidic devices. Nat Commun 2013;4:1994.
[97] Okawachi Y, Bigelow MS, Sharping JE, Zhu Z, Schweinsberg A, Gauthier DJ, Boyd RW, Gaeta AL. Tunable all-optical delays via Brillouin slow light in an optical fiber. Phys Rev Lett 2005;94:153902.
[98] Rodgers BC, Russell TH, Roh WB. Laser beam combining and cleanup by stimulated Brillouin scattering in a multimode optical fiber. Opt Lett 2999;24:1124–6.
[99] Li J, Lee H, Chen T, Vahala KJ. Characterization of a high coherence, Brillouin microcavity laser on silicon. Opt Express 2012;20:20170–80.
[100] Kalosha VP, Li W, Wang F, Chen L, Bao X. Frequency-shifted light storage via stimulated Brillouin scattering in optical fibers. Opt Lett 2008;33:2848–50.
[101] Schuller JA, Barnard ES, Cai W, Jun YC, White JS, Brongersma ML. Plasmonics for extreme light concentration and manipulation. Nat Mater 2010;9:193–204.
[102] Lorente-Crespo M, Wang L, Ortuño R, Garcia-Meca C, Ekinci Y, Martinez A. magnetic hot spots in closely spaced thick gold nanorings. Nano Lett 2013;13:2654–61.
[103] Kelf TA, Tanaka Y, Matsuda O, Larsson EM, Sutherland DS, Wright OB. Ultrafast vibrations of gold nanorings. Nano Lett 2011;11:3893–8.